POLITECNICO DI TORINO

BACHELOR DEGREE IN
ELECTRONIC ENGINEERING

INTERNSHIP REPORT

A Long-Range Digital Acoustic Thermometer

ALESSANDRO SPATARO
Advisors: ***Marco Pisani, Giovanni Ghione***
4/10/2021
01/12/2021

ANDREI GHEORGHIU
Advisors: ***Marco Pisani, Franco Fiori***
08/09/2021
08/12/2021

Summary of the internship activity

The internship took place at the Italian National Metrology Institute (INRiM - Istituto Nazionale di Ricerca Metrologica) on Strada delle Cacce 91 (Turin) between September 8th 2021 and *insert end date* for Andrei Gheorghiu and between October 4th 2021 and December 1st 2021 for Alessandro Spataro). We start this report with a brief background presentation of the institute.

INRIM is a public research centre and is Italy's national metrology institute (NMI). INRIM realises, maintains, and develops the national reference standards of the measurement units of the International System (SI), consisting of seven base units - metre, kilogram, second, ampere, kelvin, mole, and candela - and derived units. Thanks to these standards, the Institute ensures measurements that are reliable and comparable on both a national and international scale. INRIM's research spans many other areas such as materials science, nanoscience, quantum optics, studies on the fundamental constants of physics. Basic and applied research and the development of new measurement technologies and instruments enhance the metrology activity. Through seminars, exhibitions, events and conferences, INRIM presents and disseminates its scientific findings and advancements. The Institute promotes education and training for young scientists organising PhD courses and financing scholarships and research grants. To meet the needs of industry, INRIM has a dedicated department working in close contact with the world of production and providing consultancy, calibration, and testing services. The Institute supports the National Laboratory Accreditation System by ensuring the quality of measurement standards and procedures and promoting the dissemination of the national standards of the SI measurement units.

The first internship to start was that of A.Gheorghiu on September 8th. He was assigned to help an intern colleague working on a project which would later be the main topic of both internships. The project consisted of building an acoustic thermometer for long distances (with a final goal of 200 meters) using a method of phase tracking a transmitted carrier and converting the unwrapped phase over time into speed of sound and subsequently into temperature, starting from the initial phase cycles due to the distance between the microphone and the speaker. The velocity as a function of initial phase and real time unwrapped phase is $v_s = \frac{D \cdot f}{\Phi + \Phi_0}$ where D is the distance, f the frequency, Φ the phase and Φ_0 the initial phase difference. He spent the first month working on the equipment, building a tweeter array to use as a transmitter, doing directivity measurements of the array and microphone. At the end of september the first tests with the phase tracking system were carried out. One specific test was done at 18kHz over one entire weekend and it showed that the system for unknown reasons can lose track of the previous phase cycles and increase to an unrealistic value over a short period of time. After this error the system kept following the temperature reference with a certain constant error, but at unrealistic values (e.g. 90°C). The experiments proved that the phase tracking system was very sensible to disturbances like wind and went into unrecoverable errors.
In the mean time A.Gheorghiu thought of a totally different approach to this problem and came up with a new system idea which could possibly be much more robust and resistant to wind & turbulence by virtue of being entirely digital in principle. The method consisted of sending short acoustic pulses of a certain frequency and obtain the time delay between the time at which the pulse was sent and the time the system received it, to calculate the flying time of the acoustic wave which would give the average speed of sound over that portion of air. And exactly like the previous system, convert that speed of sound to temperature. To do this we decided to use an On-Off-Keying modulation scheme, to multiply a high frequency carrier with a modulating square wave going between a certain voltage to 0V, giving periods where the signal would be zero, and periods where the signal would be identical to the carrier.

Once the OOK modulated signal traveled through the air and got to the microphone the Data Acquisition System would sample and quantize this signal and send it to the Digital Processing System which in our case was the LabView software running on a personal computer. During this time in the beginning of October, A.Spataro started his internship (October 4th).

For a few days A.Spataro worked on analyzing data from the previous experiment but soon started to work together with A.Gheorghiu at the new system. Together we began to build the LabView software which would do the necessary digital processing to demodulate the received signal and extract the time information from it. This was a long process which would continue for both until the end of the internship. We worked on the first version of the program for the better part of October and on Oct. 25th the first functional version was working. The first measurement lasted 933 minutes (15.5 hours) producing one temperature value per second.The data plot showed that the system was still prone to making a high number of errors over long periods of time. However, the plot retained most of the important information and was still readable even without processing of the data. This result was already an improvement compared to the previous system were errors shifted the temperature permanently and could not be localized to one sample in time, while in this case errors were local and after an error took place the next values would always go back to the "true" states. To stop those clearly wrong values to be registered on the plot, we worked on implementing an error correction algorithm on which we improved for a long time up until the end of November. The error correction was based on rejecting values which shifted too much from the previous or a moving average of a number of previous registered values, replacing the rejected measurement with the previous accepted value already on the temperature plot. During this time the standard distance of all measurements was around 43 meters.

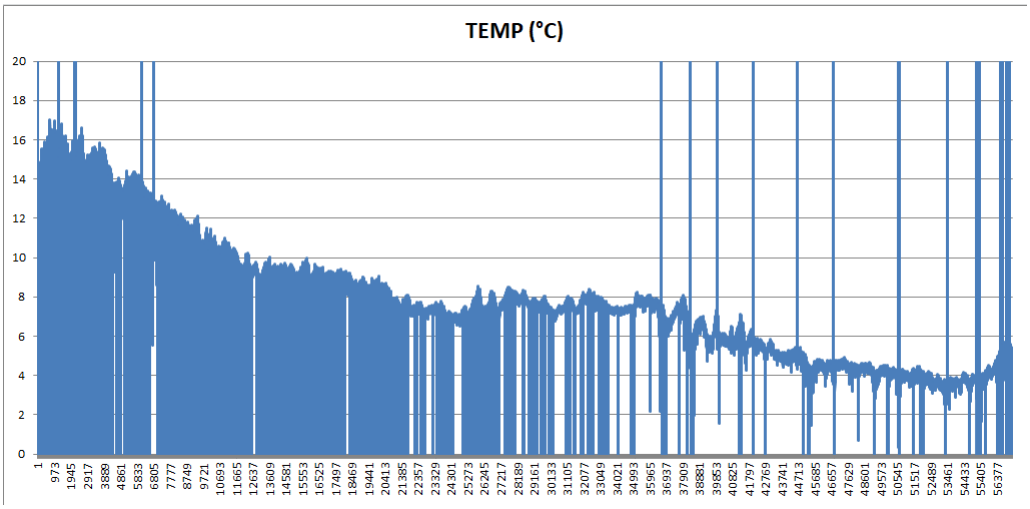

Fig.1 - First temperature measurement

Another problem was the chaotic amplitude oscillation and envelope distorsion of the demodulated signal (the signal on which the triggering is applied) owing to the way air diffracts sound waves at large distances due to wind and temperature gradients, creating interference at the microphone position and sometimes even canceling the signal altogether. This oscillation caused an uncertainty in the time delay when the trigger was fixed to a certain voltage value, a kind of noise added to the time difference. To solve this problem we came up with a dynamic threshold which adjusts the threshold level in real time by considering the amplitude of the demodulated waveform and setting the voltage level to a certain percentage of that amplitude.

In parallel to this we decided to build a low-noise pre-amplifier for a new passive electret microphone to use it together with a parabola to try and possibly capture more signal at high distances. The amplifier worked but given the need to power it to a dual rail we figured that it wasn't such a large improvement compared to the portable microphone and in the end didn't use it for most of our later measurements.

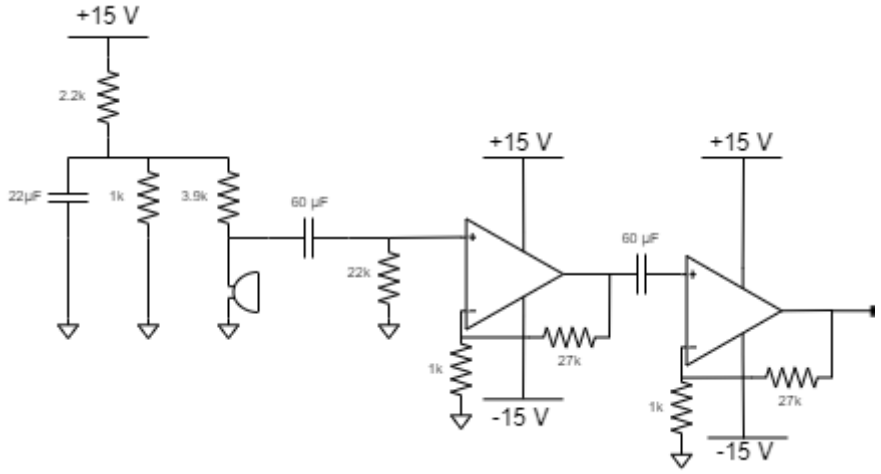

Fig.2 - Low Noise Amplifier Circuit

After a series of improvements to the program in November we decided to test the system in controlled conditions where there would be no wind and the temperature would be relatively constant, so we brought the speaker and microphone inside the building and placed them in our room at a distance of approximately 5 meters. The results showed the inherent uncertainty of the system which was around 0.3 degrees without the error correction algorithm and around 0.18 degrees with the error correction activated. A few days later the system was brought back outside but at a lower distance of 5 meters. We did a lot of tests at this distance and observed that the uncertainty with which we measure the distance is much more relevant at short distances and that how we handle the laser telemeter with which we measured the distance was giving an uncertainty which became large enough at short distance to produce changes of a few degrees in temperature.

Regarding the way we compared our results to other thermometers, during the whole project we used 4 different references, some more than others. The first reference was a station placed right outside our building which would measure the temperature and send it to a computer with one sample per second, we later connected some wires to the internal circuitry of the station to get the analog voltage representing the temperature and sample it using our DAQ system and integrate it into LabView. Another reference was the meteo station from INRiM which we consulted regularly for data on humidity, pressure and temperature, but with a low time resolution and with no way to integrate it into the system to do any statistical analysis. The last two references were one handheld thermometer device and one circuit we built using the LM35 integrated temperature sensor.

At the end of the internship we reached the goal of doing a long time measurement at a distance of 200 meters. A comparison with other instruments of this kind is yet to be done as of December 8th 2021.

In this internship we used a lot of knowledge from different courses to independently build an instrument capable of reliable measurements. We applied knowledge learned in Physics, Signal & Communication Theory, Analog & Power Electronics and Programming. Aside from an opportunity to apply knowledge from a lot of different fields to build a working and complete system, this internship was a great learning opportunity with regard to the problems arising when working in the real world and how to approach problem solving in a real research environment. We learned to properly use different kinds of measurement equipment, become more acquainted with software tools like LabView and Excel, build circuits & find solutions to different problems arising "on the field", sometimes unexpected and entirely practical but nonetheless very important when working on a research project.

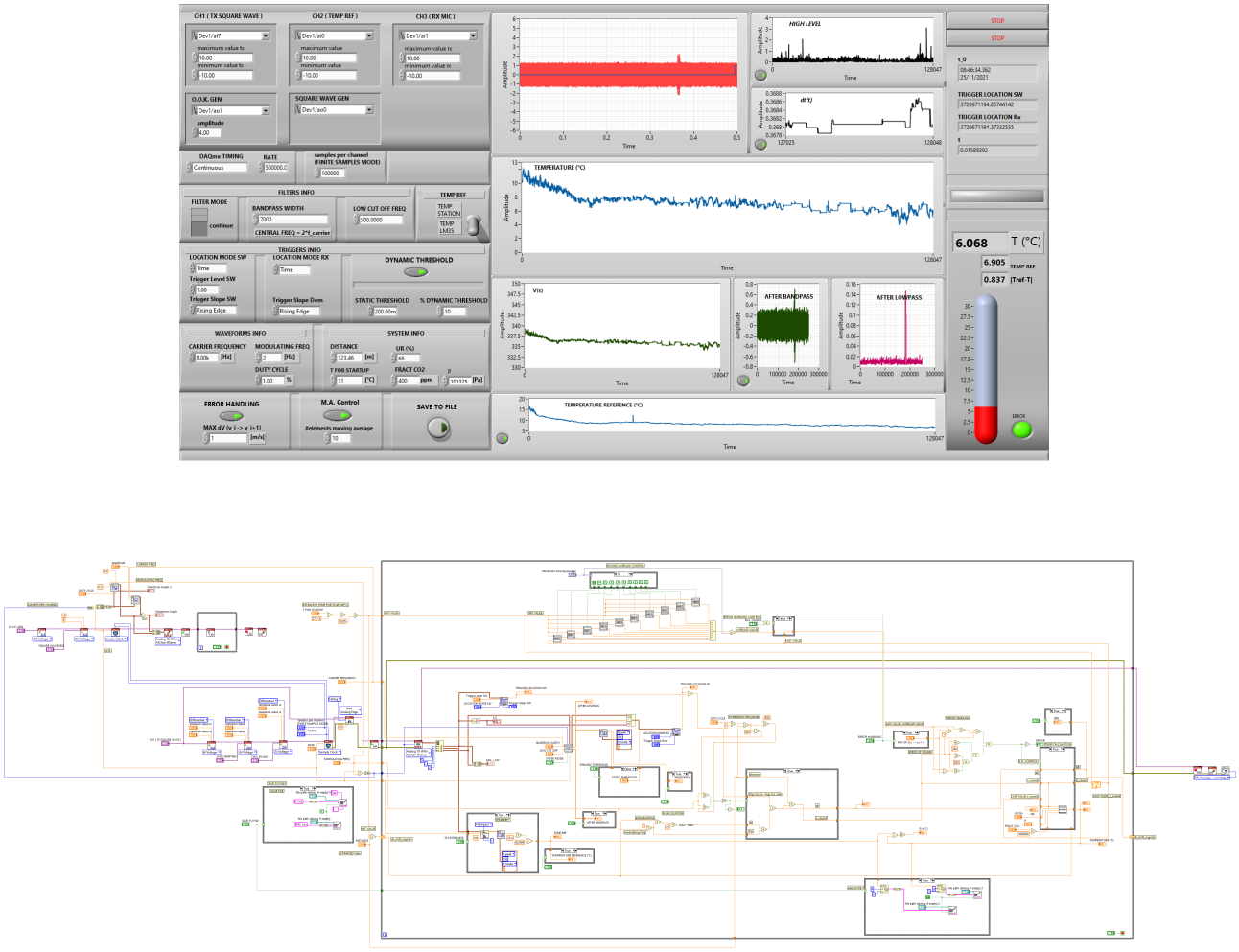

Fig.3 - LabView Software Interface and Block Diagram.

A Long-Range Digital Acoustic Thermometer

A. Spataro and C.A. Gheorghiu

Istituto Nazionale di Ricerca Metrologica (INRiM), Turin, Italy
Politecnico di Torino, Turin, Italy

December 2021

Abstract — In open air interferometric distance measurements with sub-micrometer accuracy requirements the refractive index of air becomes an important factor in the measurement of the distance. The refractive index depends on many environmental parameters but the most important and most variable locally is temperature. This project consisted in the development of a long range digital acoustic thermometer capable of measuring the real-time average temperature of a mass of air influenced by turbulence & wind over distances of up to two hundred meters with an absolute uncertainty of less than one Kelvin when compared to standard thermometers .

I Working principle

The principle of this measurement method is based upon the calculation of the average speed of sound over a large portion of air between a transmitter-receiver pair found at a distance of 5 to 200 meters. The speed is afterwards converted to temperature using Cramer's formula[2].

Our method is thus concerned with finding the average speed of sound in air when disturbances by wind & turbulence are not negligible.A sinusoidal carrier (usually at high frequencies) is modulated by On-Off-Keying with a low-frequency square signal (2-20Hz typical with duty cycle of less than 20%) the resulting waveform is amplified and fed into a speaker where it propagates and reaches the receiving side of the system (a microphone) to be then amplified again and processed digitally to obtain the time delay between the rising edge of the modulating waveform and the rising edge of the OOK demodulated signal.

The time delay is converted into speed of sound by the simple relation $v_s = \frac{d}{\Delta t}$ where d is the distance between the transmitter and the receiver. In the following paragraphs we will describe the process of modulation and demodulation with a brief spectral analysis. Some notation clarifications: We use $u(t)$ to denote the Heaviside step-function. $\mathcal{P}_x(f)$ to denote the spectral power density of a signal $x(t)$.

A.Modulation

Let $x_c(t)$ be the carrier to be modulated by $x_m(t)$ where D_c is the duty cycle and $T_m = \frac{1}{f_c}$.

$$x_c(t) = A\cos(2\pi f_c t + \phi)$$
$$x_m(t) = \sum_{n=-\infty}^{+\infty} u(t - nT_m) - u(t - (D_c + n)T_m)$$

The multiplication result becomes a convolution between the Fourier transforms of the signals in the frequency domain. We also know that $x_m(t)$ can be written as the convolution product between the element of the sum when $n = 0$ and a dirac delta train of period T_m denoted by $\mathrm{III}_{T_m}(t) = \sum_{n=-\infty}^{+\infty} \delta(t - nT_m)$.

$$x_{TX}(t) = x_c(t) \cdot x_m(t) \xrightarrow{F} \tilde{X}(f) = X_c(f) * X_m(f)$$
$$X_c(f) = F\{x_c(t)\} = \frac{A}{2}[e^{j\phi}\delta(f - f_c) + e^{-j\phi}\delta(f + f_c)]$$
$$X_m(f) = F\{[u(t) - u(t - D_c T_m)] * \mathrm{III}_{T_m}(t)\}$$
$$= \frac{\sin(\pi f D_c T_m)}{\pi f} e^{-j\pi f D_c T_m} \cdot \frac{1}{T_m}\mathrm{III}_{\frac{1}{T_m}}(f)$$
$$X_{TX}(f) = \frac{A}{2}X_m(f) * [e^{j\phi}\delta(f - f_c) + e^{-j\phi}\delta(f + f_c)]$$

Having signals of disjoint support in the Fourier domain and knowing that $e^{\pm j\phi}$ does not depend on frequency (so the product and convolution can be interchanged), we can write the PSD $\mathcal{P}_x(f) = |\tilde{X}(f)|^2$ as follows:

$$\mathcal{P}_{TX}(f) = |\tfrac{A}{2}[e^{j\phi}X_m * \delta(f - f_c) + e^{-j\phi}X_m * \delta(f + f_c)]|^2 \approx$$
$$\tfrac{A^2}{4}[|X_m(f) * \delta(f - f_c)|^2 + |X_m(f) * \delta(f + f_c)|^2]$$

Even if $X_m(f)$ does not have a finite support we can still make this approximation knowing that the spectrum magnitude vanishes in the limit of $f \to \pm\infty$. Finally the PSD of the O.O.K. modulated signal to be transmitted can be written as:

$$\mathcal{P}_{TX}(f) = \frac{A^2}{4}[|X_m(f - f_c)|^2 + |X_m(f + f_c)|^2] \quad (1)$$

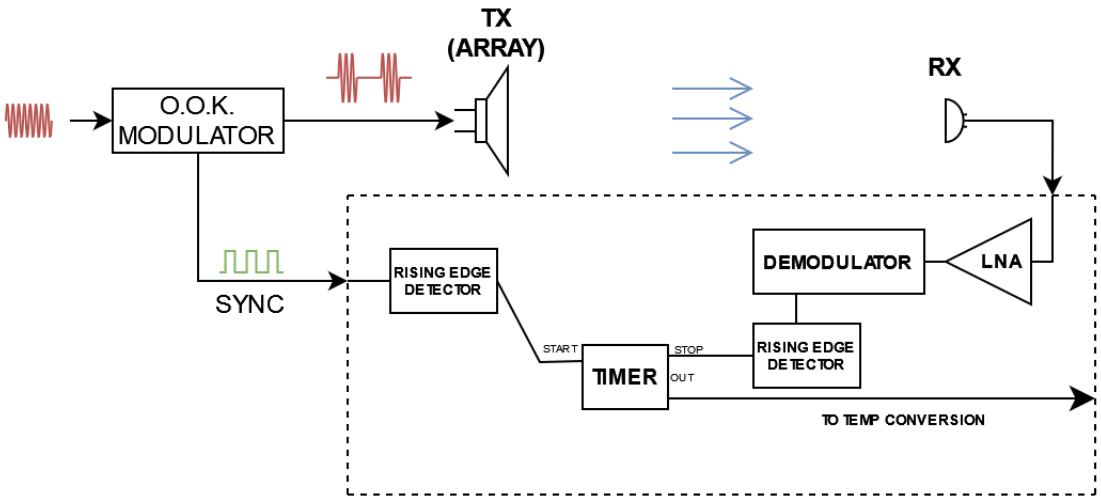

Fig.1.1 - Functional block diagram of the system (simplified timing)

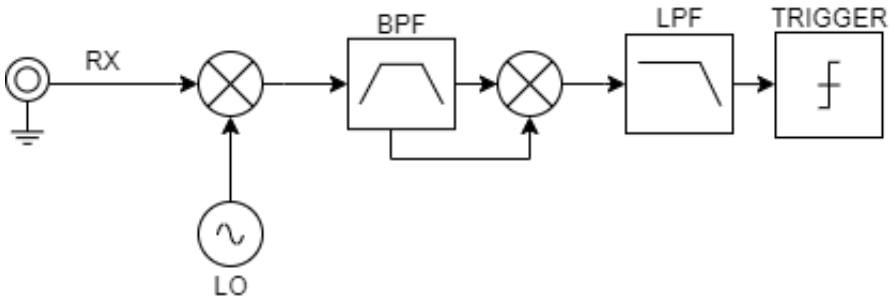

Fig.1.2 - Diagram of the OOK demodulator

B. Demodulation

Once transmitted the signal is influenced by dispersion and non-linear distorsion due to chaotic variations of air density, wind and turbulence. The mathematical analysis of those effects are outside the scope of this study as our system actively detects and avoids conditions where these non-linear effects change the time delay by a significant margin (section II.A). Qualitatively we expect smaller wavelength components to be attenuated more than larger wavelength components. The signal is received and amplified by a low-noise amplifier before entering the demodulation phase (Fig.2).Let the received PSD be $\mathcal{P}_{RX}(f)$.

The received signal is mixed with a sinusoid produced by the a local oscillator at the same frequency of the carrier (no phase locking). The product is filtered by a bandpass filter centered around $2f_c$ and mixed again with itself. Now a DC component is present in the signal and can be filtered by a low-pass filter to give a signal which can regenerate the modulating digital signal after passing through a rising edge detector. The values chosen for the filters and trigger are very important and will be discussed along with their influence over the system response in later chapters.

$$x_{LO}(t) = \cos(2\pi f_c + \phi_{LO})$$

$$\mathcal{P}_{RX}(f) = \frac{B^2}{4}[|X_m(f - f_c)|^2 + |X_m(f + f_c)|^2]$$

$$\mathcal{P}_{LO}(f) = \frac{1}{2}[\delta(f + f_c) + \delta(f - f_c)]$$

$$\mathcal{P}_{LO} * \mathcal{P}_{RX} \propto |X_m(f)|^2 + |X_m(f - 2f_c)|^2 + |X_m(f + 2f_c)|^2$$

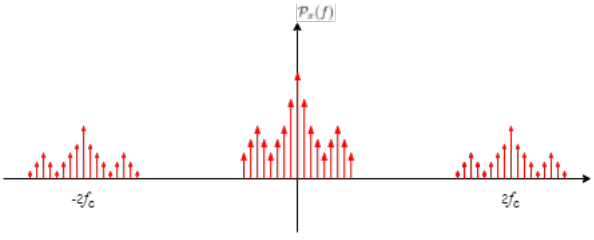

Fig.1.3 - Qualitative graph of the demodulated PSD

C. Triggering and Time Measurement

After demodulating the signal and obtaining a PSD of the type seen in the last equation we can low-pass filter it and select a proper threshold voltage for the rising edge detection. The cut-off frequency of the LPF determines the speed at which the rising edge of the signal reaches the threshold and with it an intrinsic time delay between detection and demodulation. As the cut-off frequency gets smaller the signal gets cleaner with less oscillations and band noise but the edge gets triggered later as the slew rate gets smaller. We balance this trade-off by experimental trial and error to obtain a waveform which can be triggered but is not too slow. The uncertainties involved are analyzed below.

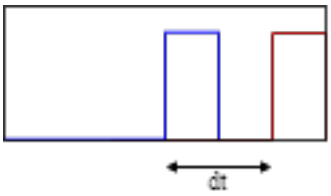

Fig.1.4 - Time delay between the modulating signal and digital trigger output

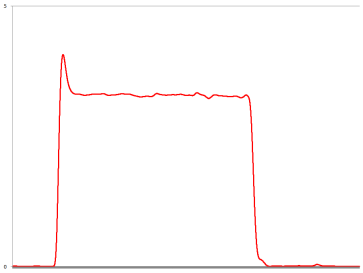

Fig.1.5 - Signal waveform after low-pass (distance around 5m)

As an example let the software delay of the demodulator be equal to $\Delta t_{AQ} = 2\mu s$ (due to data acquisition time), the distance be $d = 10m$ and speed of sound $v_s = 340m/s$ and let the demodulated signal be piece-wise linear with a slew rate of $33mV/\mu s$. The fly time of the acoustic signal in air will be approximately $\Delta t_s = 29.4ms$. Supposing the amplitudes are $1V$ each and a static threshold voltage $V_T = 0.5V$, the time delay between demodulation completion and triggering will be $\frac{0.5V}{33mV/\mu s} \approx 15.15\mu s = \Delta t_\epsilon$. Thus the total effective delay is:

$$\begin{aligned}\Delta t &= \Delta t_s + \Delta t_{AQ} + \Delta t_\epsilon \\ &= (29.4ms + 2\mu s) + 15.15\mu s = 29.42ms\end{aligned}$$

$$v_{eff} = \frac{10m}{29.432ms} = 339.9m/s$$

Giving a temperature (to first order):

$$Using: v_s = 20.05\sqrt{T} \quad (1.1)$$

$$T_{eff} = \frac{v_{eff}^2}{20.05^2} \cong 287.17K \cong 14.24°C$$

$$T = \frac{v_s^2}{20.05^2} \cong 287.56K \cong 14.41°C$$

$$\epsilon_T = T - T_{eff} = 0.17°C$$

From this calculation we notice that a 0.1% change in the time delay can produce significant temperature changes in the order of the tenth of a degree.

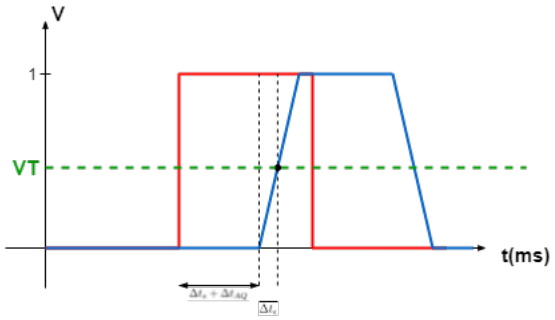

Fig.1.6 - Timing graph depicting the modulating waveform in red and the demodulated waveform in blue (not to scale)

Below we analyze the uncertainty of the simplified model using a first order approximation for the temperature dependence of velocity and the absolute uncertainty formula.

$$\delta f = \sqrt{(\frac{\partial f}{\partial x_1}\cdot\delta x_1)^2 + (\frac{\partial f}{\partial x_2}\cdot\delta x_2)^2 + ... + (\frac{\partial f}{\partial x_N}\cdot\delta x_N)^2}$$

$$\delta\Delta t = \sqrt{\frac{(d\cdot\delta T)^2}{(2\cdot 20.05T^{\frac{3}{2}})^2} + \frac{(\delta d)^2}{(20.05\sqrt{T})^2}} \quad (2)$$

Knowing that our uncertainty in temperature must not be greater than one celsius degree, and that the uncertainty due to the handling of the laser telemeter used is around ten centimeters at maximum, we can estimate the variation in time delay. We also calculate the maximum time delay error at a distance of 50m and at a temperature of 290K to get $\Delta t_{MAX} \cong 296ms$.

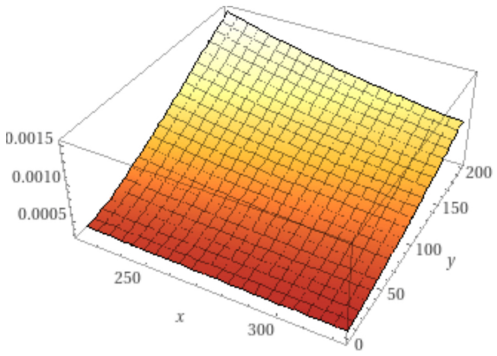

Fig.1.7 - Graph of the maximum variation in time delay as a function of temperature (x Kelvin) and distance (y meters)

By fixing our allowed uncertainty in temperature to 1 K and considering a range of distances from 5 to 200 meters we can calculate (using equation [3]) the maximum demodulation time to obtain an accurate measurement over the whole range of possible temperatures (-50° C to 50° C).

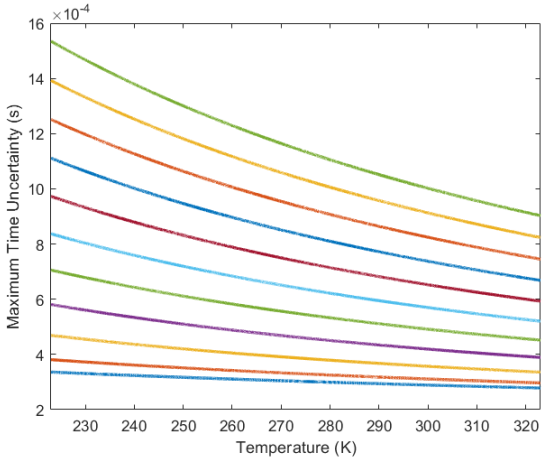

Fig.1.8 - Time delays as functions of temperature (distance increases with the positive vertical direction)

At 300K we get a time uncertainty of $\delta\Delta t_{MIN} = 289\mu$s for a distance of 5 meters and an uncertainty of $\delta\Delta t_{MAX} = 1000\mu$s at 200 meters. Translated into relative uncertainties they are:

$$\frac{\delta\Delta t_{MIN}}{\Delta t_{MIN}} = \frac{289\mu s \cdot (20.05\sqrt{300K})}{5m} = 0.0200 \ \ (2\%)$$
$$\frac{\delta\Delta t_{MIN}}{\Delta t_{MIN}} = \frac{1000\mu s \cdot (20.05\sqrt{300K})}{200m} = 0.0017 \ \ (0.17\%)$$

D. Power Considerations

On the transmitting side our system uses a signal generator feeding an amplifier which transmits the signal along a shielded cable to the speaker, assuming a gain $A_v = 7.5V/V$, a maximum peak transmitted power of 100W, a 4Ω speaker, a total series impedance seen by the amplifier of 20Ω, we calculate the average power delivered by our modulation scheme and find the voltage needed (at the signal generator) to send 100W of peak power, we then compute the average power over one modulation period.

$$v(t) = V\cdot\cos(2\pi f_c t)\cdot[u(t) - u(t - D_c T_m)]$$

$$V_{RMS} = \sqrt{\frac{1}{T_m}\int_0^{T_m}[V_p\cdot\cos(2\pi f_c t)\cdot(u(t) - u(t - D_c T_m))]^2 dt} = \sqrt{\frac{1}{T_m}\int_0^{D_c T_m}[V_p\cdot\cos(2\pi f_c t)]^2 dt} =$$

$$= \sqrt{\frac{1}{T_m}\int_0^{D_c T_m} V_p^2\cdot\cos^2(2\pi f_c t)\,dt} = V_p\sqrt{\frac{1}{T_m}\int_0^{D_c T_m}\cos^2(2\pi f_c t)\,dt} =$$

$$= \frac{V_p}{\sqrt{2}}\sqrt{\frac{1}{T_m}\int_0^{D_c T_m}(1 + \cos(4\pi f_c t))\,dt} = \frac{V_p}{\sqrt{2}}\sqrt{D_c + \frac{1}{T_m}\int_0^{D_c T_m}\cos(4\pi f_c t)dt} =$$

$$= \frac{V_p}{\sqrt{2}}\sqrt{D_c + \frac{1}{T_m}\left[\frac{1}{4\pi f_c}\sin(4\pi f_c t)\right]_0^{D_c T_m}} = \frac{V_p}{\sqrt{2}}\sqrt{D_c + \frac{1}{4\pi f_c T_m}\sin(4\pi f_c D_c T_m)} \quad (3)$$

The cable and the speaker compose a voltage divider, using the values stated above we get a voltage across the speaker of $V_A \cong 0.15\cdot A_v V_p$. We set the average power of the sinusoid $P_{peak} = \frac{(V_A/\sqrt{2})^2}{4} = 100W$ resulting in $V_p \cong 25.14V$. implying $V_A = 28.28V$ as a peak voltage. With these values we now use equation (3) to find an average transmitted power of $P_{av} = \frac{(0.32V_A)^2}{4} = 20.5W$. The 0.32 term multiplying V_A comes from evaluating equation (3) at $D_c = 0.2; f_c = 18kHz; V_p = 1V$ and $f_m = 12Hz$.

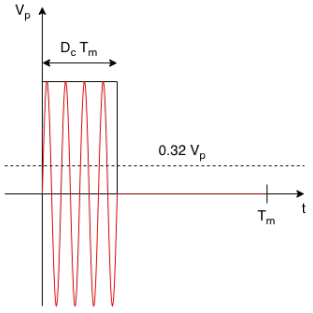

Fig.1.9 - Transmitted signal in time domain

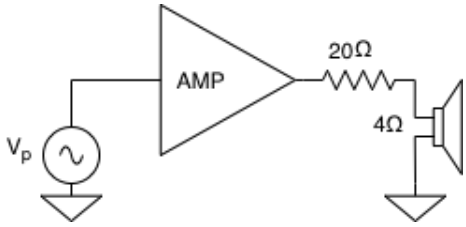

Fig.1.10 - Signal path to the speaker

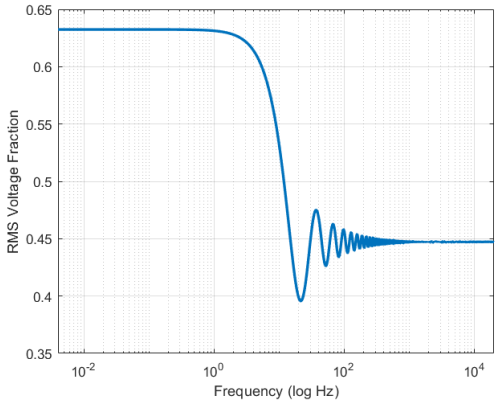

Fig.1.11 - Fraction of the non-modulated RMS Voltage at the OOK modulated output as a function of f_c

E. Influence of Wind & Turbulence

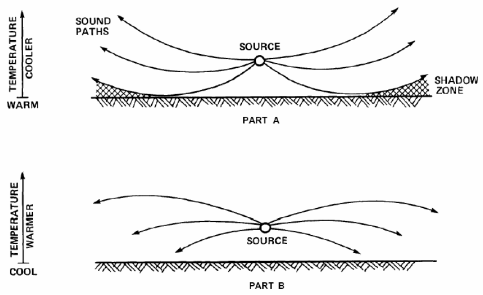

Fig.1.12

Fig.1.12 - Effects of temperature gradients on sound propagation. (Top): In the case of upward refraction (temperature decreases with height or upwind propagation) ground based layers are generated into which sound energy is not directly shed. (Bottom): Downward refraction (temperature inversion or downwind propagation) causes multiple reflections at the ground and is known as a condition that is favourable to sound propagation over long distances [3][11]

The diffraction of sound waves can be caused by vertical temperature gradients or by wind action. This phenomenon adds to the time it takes for the signal to travel from the transmitter to the receiver and cannot be corrected for as in this study we have no way to accurately measure or predict the complex movements of air masses.

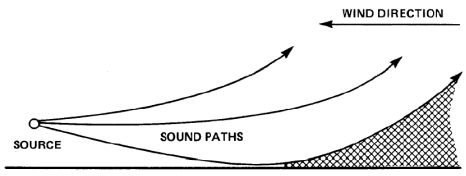

Fig.1.13 - Example of up-wind sound effects[3][9]

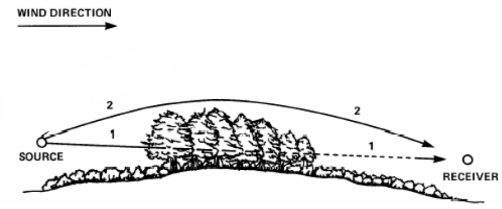

Fig.1.14 - Example of downwind sound diffraction[3][8]

Irregular, turbulent, or gusty wind provides fluctuations in sound transmission over large distances (this may be because of partial wavelength interference of various paths taken by various sound rays of the total beam) [3]. This effect was prevalent at long distances in all our experiments and was a prevalent source of errors. By decreasing the duty cycle of the modulation and using a combination of error correction algorithms and proper filtering of the signal we were able to minimize the problems associated with this effect.

II Digital Processing

The demodulation and digital processing of the data is done entirely in LabView, in the following paragraphs we explain the structure of the program and reasoning behind certain design choices.
The execution of the program starts with the data acquisition by the three physical channels: the modulating square-wave (used for the O.O.K. modulation), the temperature reference (acquired by an outdoor precision thermometer) and the received signal (acquired by a microphone).

All these inputs go into a *sample clock* (500kHz controllable sampling rate), then into a DAQmx Start Trigger that stores data from the modulating square-wave rising/falling edge. That step is really important because the program will always consider one period per cycle (the DAQmx-Read block read $\frac{rate}{freq_{mod}}$ samples per channel). In this case the program will start reading data once the modulating s.w. falling edge enters the acquisition system, allowing the trigger to detect the rising one inside the reading data package.

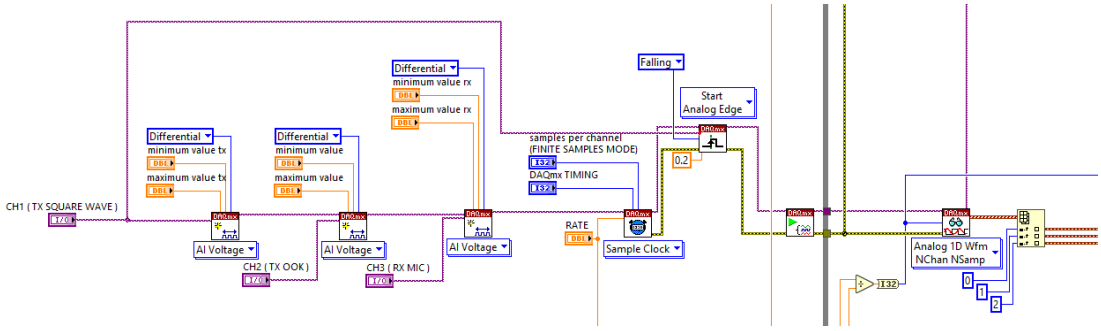

Fig.2.1 - LABView diagram - Channel inputs

The modulation of the signal to O.O.K. is also done inside the program by multiplying a square-waveform ($amplitude = 0.5$, $offset = 0.5$, controllable duty-cycle and frequency) with a sine-waveform (controllable amplitude and frequency). The generated signal comes out from two physical channels: one for the s.w. and the other one for the modulated signal.

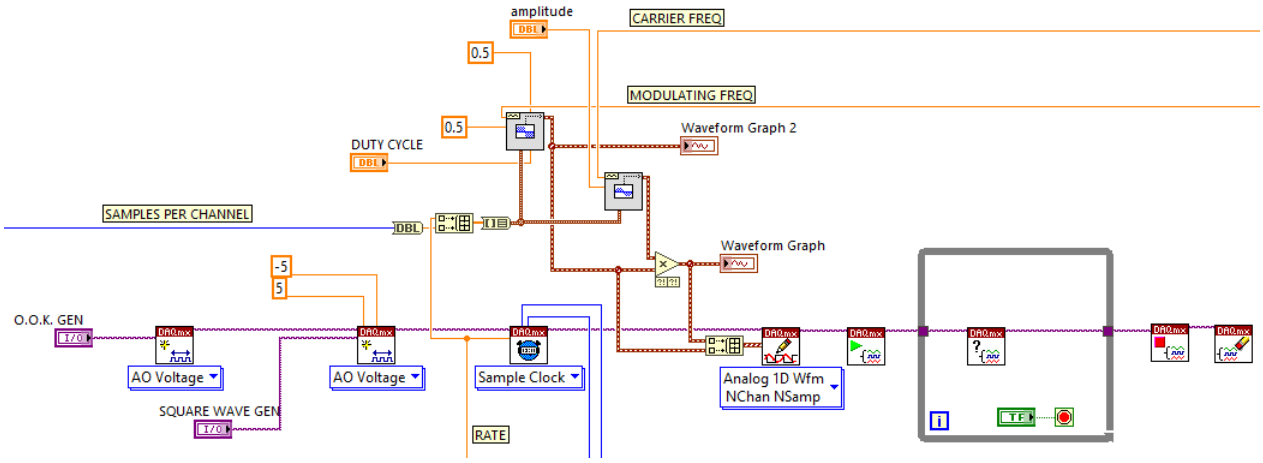

Fig.2.2 - LABView diagram - Channel outputs for the O.O.K. generation

The set up of the program needs external information to correctly execute its tasks such as an estimated temperature which will be converted to velocity: $v = 20.05\sqrt{T(°C) + 273.15}$.

This value is used as initial value for the moving average calculation algorithm (Fig. 2.14) and the estimated flying time calculation (Fig. 2.12).

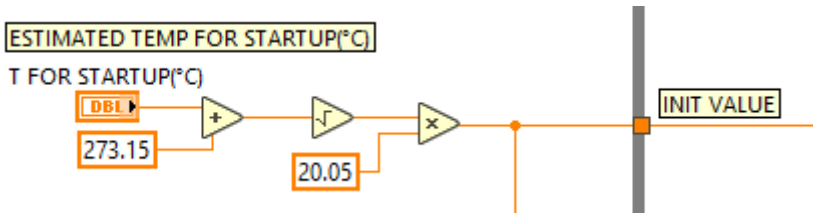

Fig.2.3 - LABView diagram - Calculation of estimated temperature for startup

The LABView diagram shown below represents the program's core, where the flying time of the acustic signal is measured by using a Basic Level Trigger Detector. This block gives as output the Julian Time (if the location mode is set as "Time") when the rising edge (trigger slope) and the amplitude level (trigger level) occur.
The first and the third input signal are respectively the demodulating square-waveform and the received O.O.K. . Both signals pass through the trigger detectors (showing the trigger locations on the program interface), except for the third one that is previously processed inside a Demodulation Block. Once this program section is executed, the difference between these two Julian Time gives an accurate time value that will be later summed up with the estimated number of periods for the specific distance and temperature the system is working on.

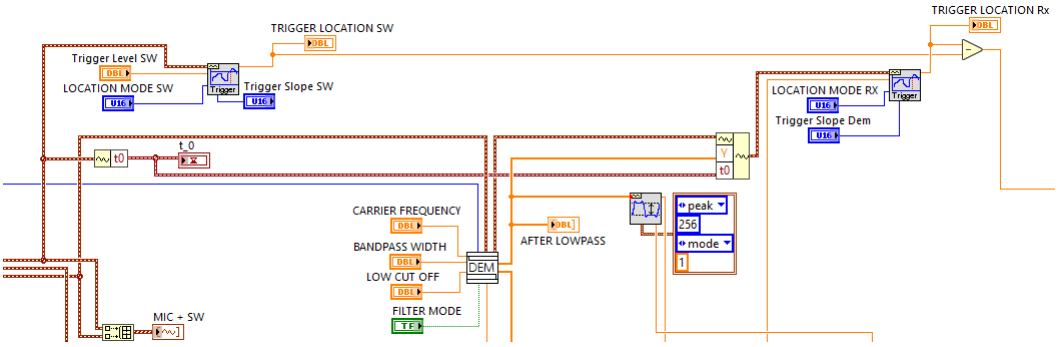

Fig.2.4 - LABView diagram - The trigger system

The Demodulation block is a LABView SubVI used to simplify the block diagram concerning the demodulation process. It includes the sine-waveform generator, two filters (Fifth Order Butterworth Bandpass, Third Order Butterworth Lowpass). It is composed by:

- **INPUT**
  - *Signal In* : the received signal enters the block to get demodulated.
  - *Samples per Channel* : an integer number (the same of the reading samples) used as information for the Sine-Waveform Generator.
  - *Freq. Sin. Dem* : an integer number (the same of the carrier frequency) used as information for the Sine-Waveform Generator.
  - *Bandpass Width*: an integer number used for the lower/upper cut-off frequency calculation of the Band-Pass Filter.

$$f_0 = 2f_{carrier}$$
$$f_L = f_0 - \frac{Bandpass\ Width}{2}$$
$$f_H = f_0 + \frac{Bandpass\ Width}{2}$$

  - *Low cut off Freq.* : an integer number used for the lower cut-off frequency of the Low-Pass Filter.
  - *Init/Cont* : a boolean value (init: F) which controls the initialization of the internal states. The default is FALSE. The first time this VI runs or if init/cont is FALSE, LabVIEW initializes the internal states to 0. If init/cont is TRUE, LabVIEW initializes the internal states to the final states from the previous call to this instance of this VI.
  - *Rate* : an integer number used for the filtering rate (the same of the *Sample Clock rate*).

- **OUTPUT**
  - *Signal Out* : the input signal leaves the block once it has been multiplied with the sine-waveform. This signal is used to get modified with new parameters: t_0 as initial time, *After Lowpass* as Y values.
  - *After Lowpass* : a double (15 digit precision) of the *After Bandpass* multiplied with itself and Lowpass filtered (*Low Cut Off Freq*).
  - *After Bandpass* : a double (15 digit precision) of the *Signal Out* Bandpass filtered (f_0, f_L, f_H).

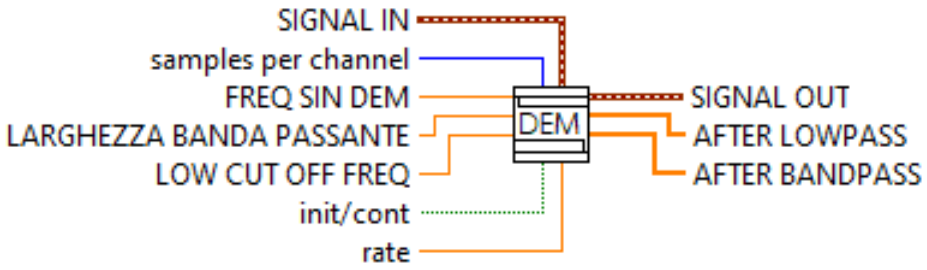

Fig.2.5 - LABView diagram - Demodulator pinout

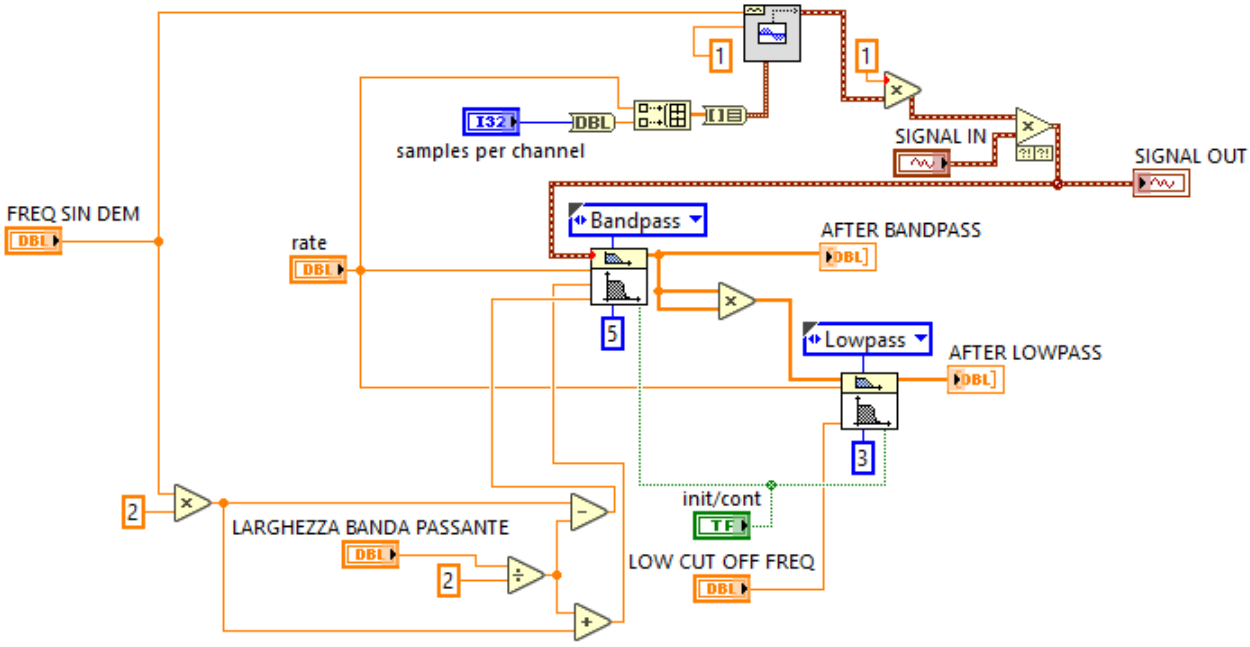

Fig.2.6 - LABView diagram - Demodulator block

The program allows to choose between a static or dynamic treshold to start the trigger of the modulated signal. Both modes are controllable by choosing respectively the amplitude value or the percentage compared with the instantaneous difference between the *High state value* (the level at which a pulse or transition waveform is defined to be in its highest state) and the *Low state level* (the level at which a pulse or transition waveform is defined to be in its lowest state).

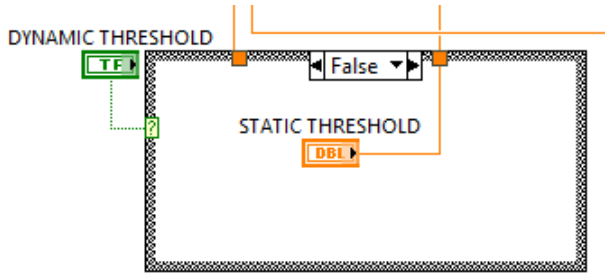

Fig.2.7 - LABView diagram - The static treshold control system

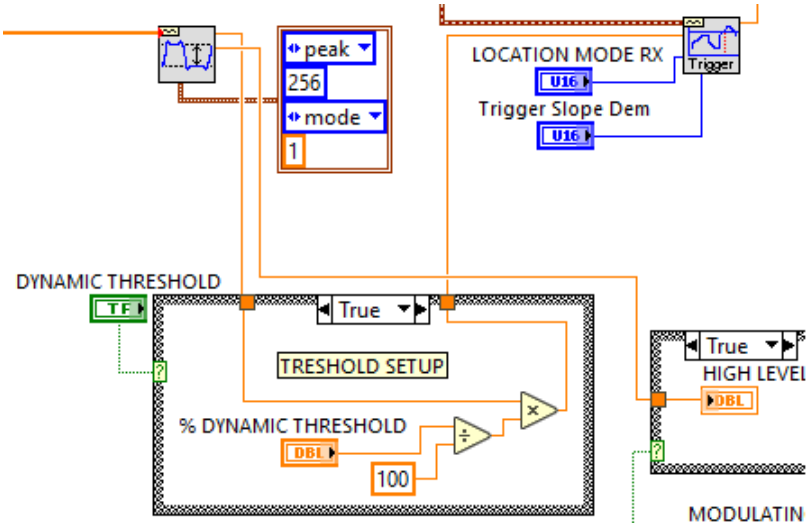

Fig.2.8 - LABView diagram - The dynamic treshold control system

The third and last physical channel is used as a temperature reference. It is possible to choose what type of reference the program will show on the front panel interface by using a toggle switch.The *FALSE* case menages a signal that comes from a small circuit using an LM35 integrated temperature sensor, filtering and scaling it by a constant factor ($10mV/^{\circ}C$). Instead the *TRUE* case menages a signal that comes from a local weather station sampling a voltage signal by filtering it and calculating the temperature by the following formula : $T(t) = 25.4 * V(t) - 65.994$. The first one has been introduced to improve the quality of the reference.

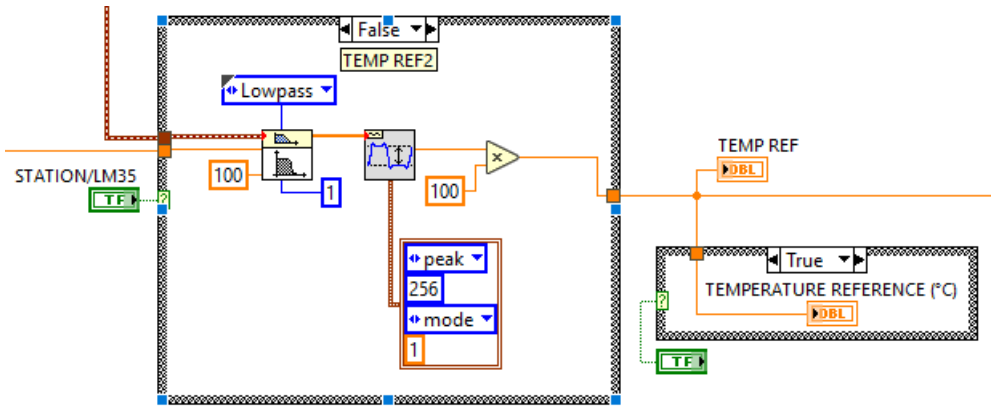

Fig.2.9 - LABView diagram - The $Tref$ calculation (False case - Thermometer with LM35).

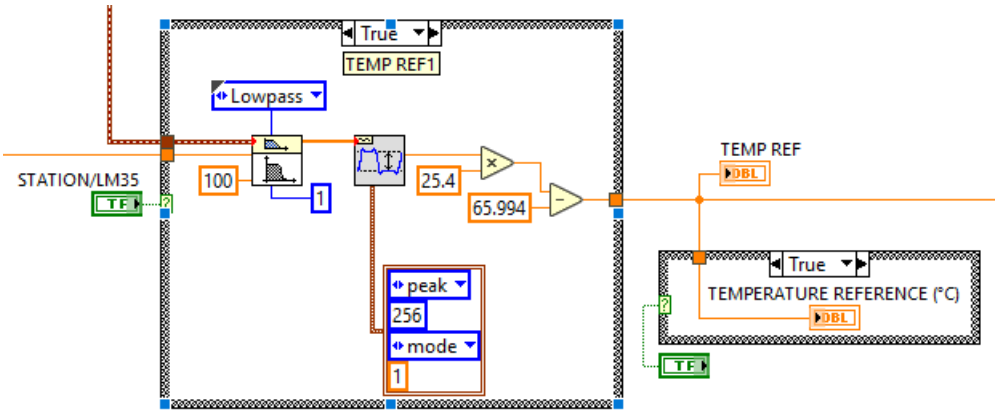

Fig.2.10 - LABView diagram - The $Tref$ calculation (True case - Local weather station).

As said before, the program needs some parameters to start measuring correctly: an estimated time and the modulating frequency are fundamental for the number of periods calculation during the flying time based on the distance. Fig. 2.11 represents the N calculation algorithm by implementing the following formula : $N = int(\frac{estimated-time}{T_m} + 0.5)$. The sum is just to be sure that N is calculated by rounding to the nearest larger integer. The periods value will be later multiplied with the modulating period and then summed up with the difference between the two trigger results. $dt = \frac{distance}{(trig.loc.rx - trig.loc.sw) + NT_m}$.

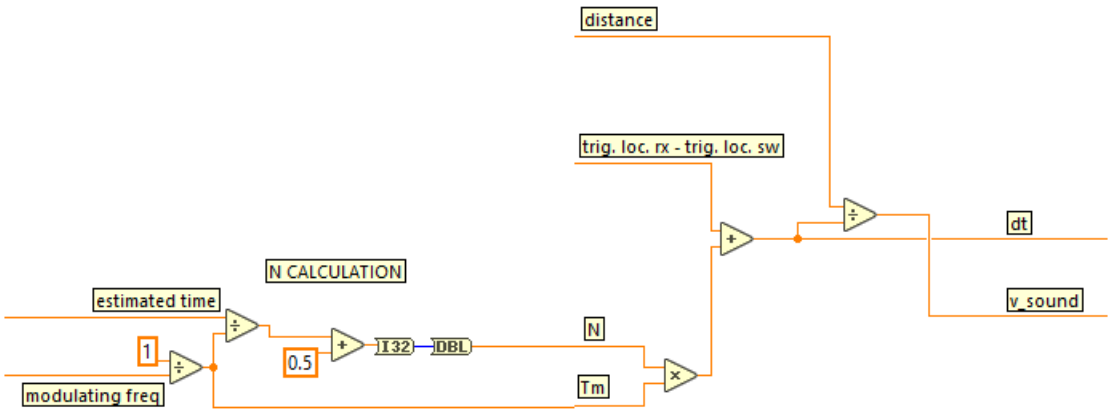

Fig.2.11 - LABView diagram - Number of periods during the flying time calculation

Fig. 2.12 represents the estimated time calculation ($time_{estimated} = \frac{v_{in}}{distance}$). It enters in the while loop as initial value and it will be updated for the next cycles thanks to a shift register.

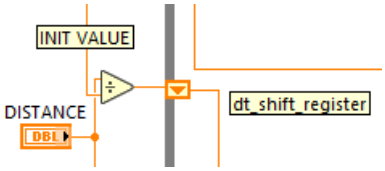

Fig.2.12 - LABView diagram - The estimated flying time calculation.

To avoid errors due to the chaotic air behaviour, the program uses a handling algorithm which ignores the acquired samples showing an increase of temperature too abrupt to be real by saving the last value instead of the false one. The error detection is based on a moving average control that takes as true values the ones which are below a maximum velocity change.
E.H. CONTROL is a boolean value that determine if the acquired data is true by the following logic function :

$$E.H.CONTROL = ((v > 300) AND (v > (AverageValue - Maxdv))) \\ AND((v < 380) AND (v < (AverageValue + Maxdv)))$$

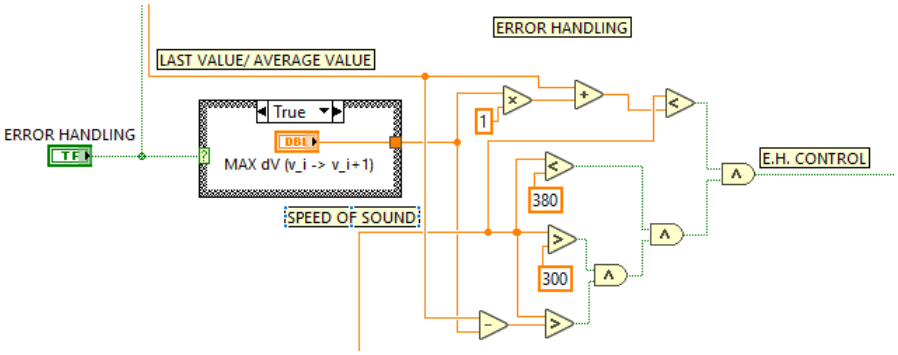

Fig.2.13 - LABView diagram - Error handling logic diagram

Maxdv is a controllable value that expresses the maximum velocity variation and *AverageValue* is an average from the 10 to 100 last velocity values by just setting *elements moving average*. The moving average control becomes active only if both the Error handling control and the moving average control are enabled.

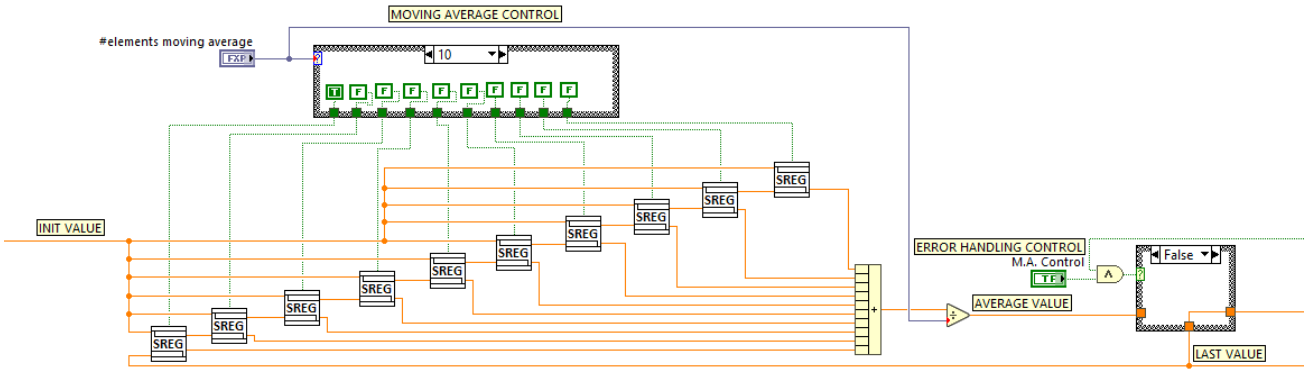

Fig.2.14 - LABView diagram - Moving average control

The SREG is the basic component of the Moving Average Control and is a SubVI that has 3 inputs (*Initial Value, Input and Enable*) and 2 outputs (*Output Value, Output Sum*). All of these blocks are connected in series and they are enabled sequentially from the left to the right according to the *elements moving average* value.
When they are disabled the *Output Sum* returns 0, otherwise the positive value is going to be summed up with the other 9 *Output Sum* values and divided by the number of considered elements.
This average evaluation (used for the error handling) is usefull to keep stable the velocity allowed band in case of multiple errors of the system calculation caused by wind/high turbulence. It is important choosing the number of elements in the moving average and the maximum velocity variation related to the modulating frequency.
It's possible to see (Fig.2.16) that each SREG block contains 10 property nodes (initialized by *Init Value*, updated by *Input* and enabled by *Enable*) that sequentially stores 10 values. The block also returns *Output Value* to properly connect the blocks in series.

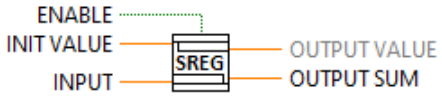

Fig.2.15 - LABView diagram - SREG pinout diagram

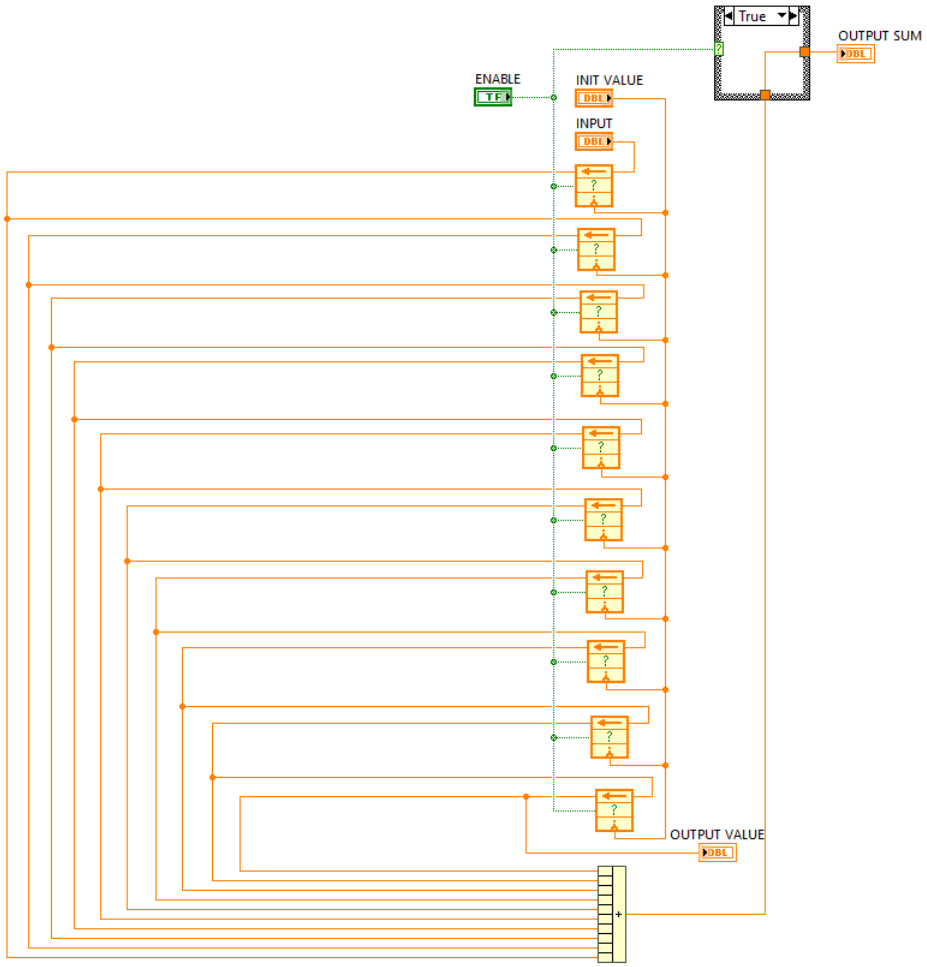

Fig.2.16 - LABView diagram - SREG block diagram

Depending on the results obtained by the previous steps there are two possibilities: either an error has been detected by the error detection circuit (setting E.H.Control to a low state) or no error has been detected (setting E.H.Control to a high state). If an error did occur the conditional structure routes the true speed of sound calculated in a previous cycle to a temperature conversion block (Cramer). Otherwise the current computed speed of sound is sent to the conversion block. In both cases the result is sent to the output of the conditional structure to be saved and displayed on the plots in the graphic interface of the program.

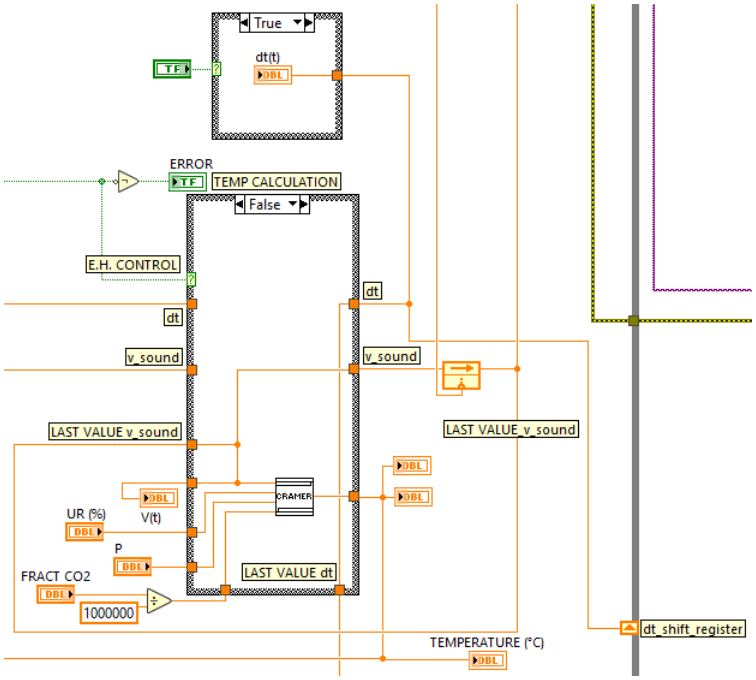

Fig.2.17 - LABView diagram - Temperature calculation (False - Error case)

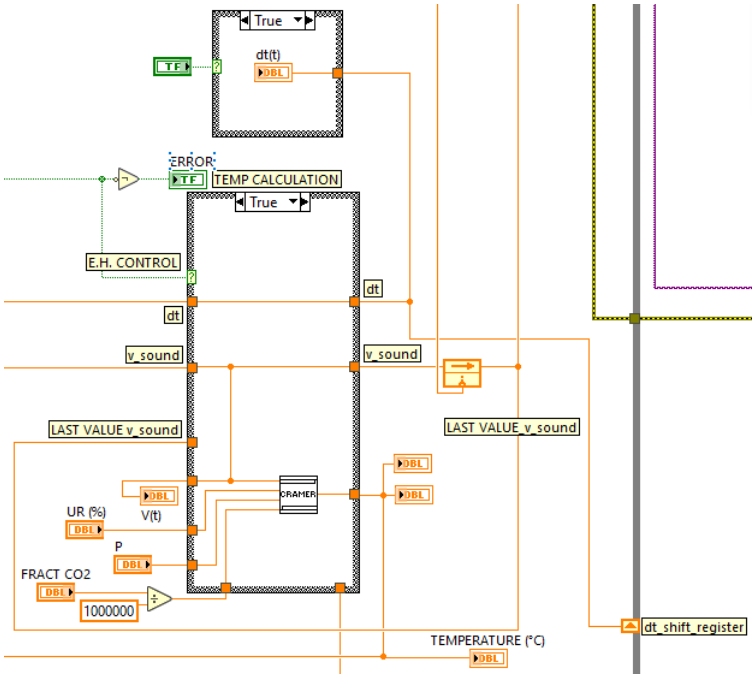

Fig.2.18 - LABView diagram - Temperature calculation (True - No Error case)

For a more precise temperature conversion Cramer's formula[2] is implemented using a formula node taking as inputs the temperature, other environmental parameters and the Cramer coefficients to calculate the speed of sound correspondent to that temperature. Given that in our context we want to do the opposite, the formula would need to be inverted. To do this we iterate from the lowest expected temperature (233.15 K) up to the point where the conversion coincides with the input speed of sound calculated by the precedent steps.

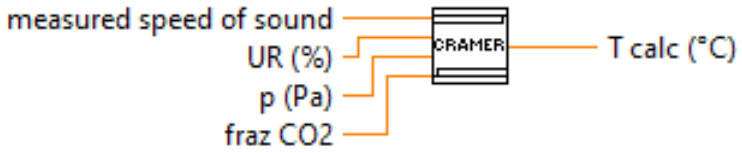

Fig.2.19 - LABView diagram - Temperature calculation

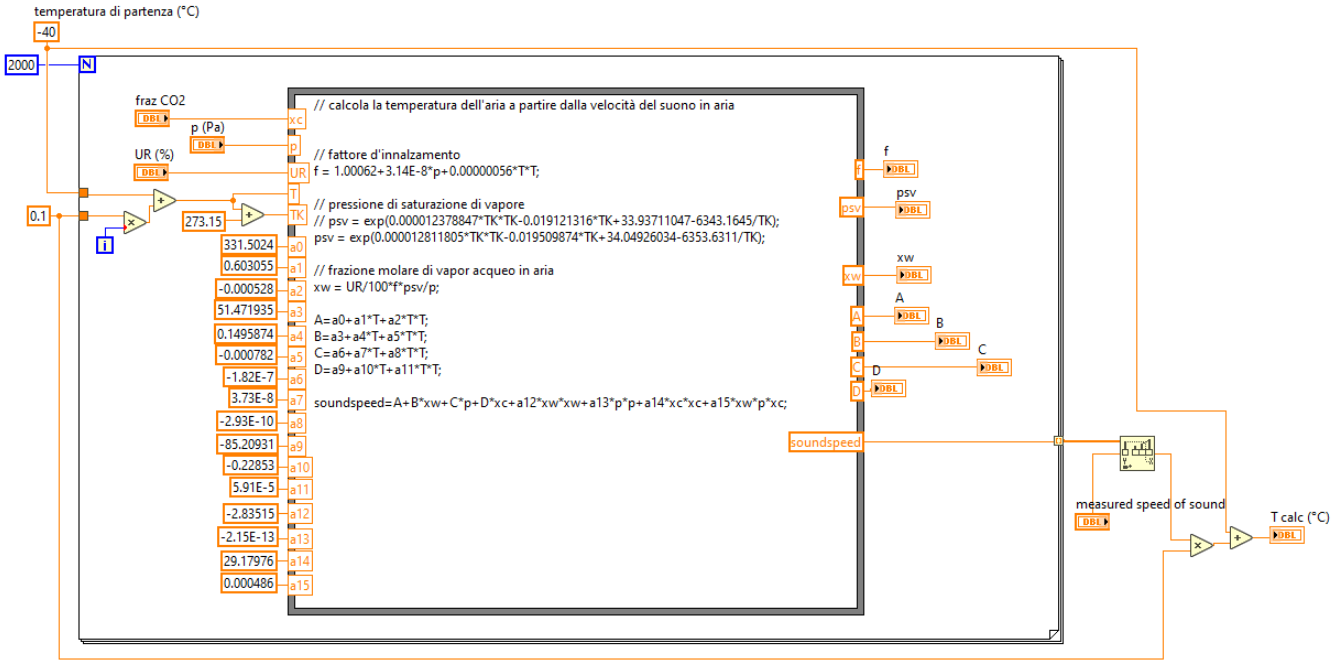

Fig.2.20 - LABView diagram - Temperature calculation

III Experimental Setup

The setup is composed of an instrument station and a microphone-speaker pair located outside on tripods.

1. Desktop computer running the LabView software
2. RIGOL DG4062 60MHz signal generator
3. Agilent MSO6104A 1GHz Oscilloscope
4. SAMSON Mix Pad 9
5. National Instruments USB 6366 X-Series Multi-function DAQ
6. GPC303RP Laboratory DC Power Supply
7. NAD Stereo Power Amplifier 912
8. ST 25A NEO ”Hertz” 100W 4Ohm Speaker
9. BOYA BY-PVM1000 Microphone

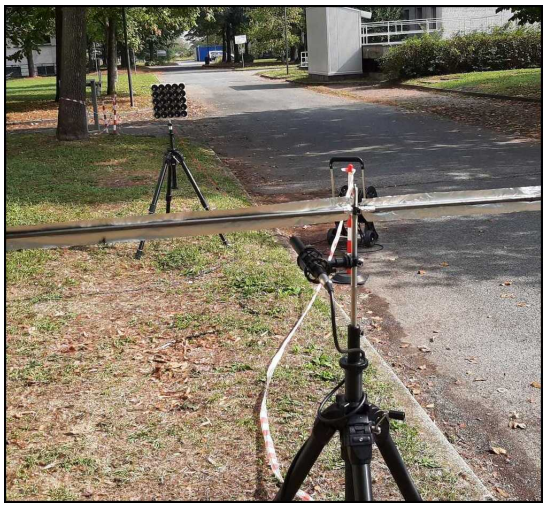

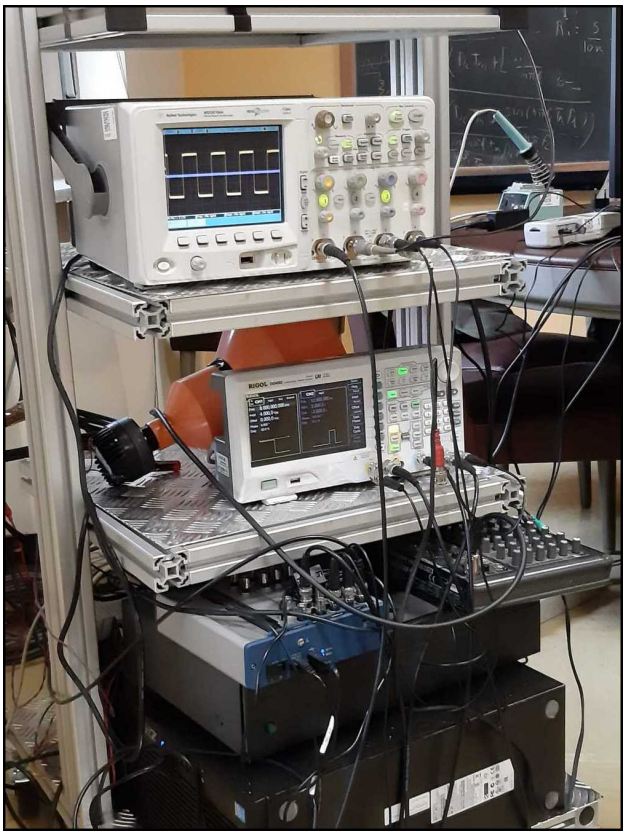

From left to right: RX-TX Pair with one 100W speaker, RX-TX Pair with a tweeter array for improved acoustic directivity, setup of the instrument station

The instrumentation station controls the speaker and receives a signal from the microphone. This signal is processed by the DAQ system and then handled digitally by the LabView software. To compare our results we use two temperature references: one is a station equipped with an internal thermometer and the other is a small circuit using the LM35 integrated temperature sensor.

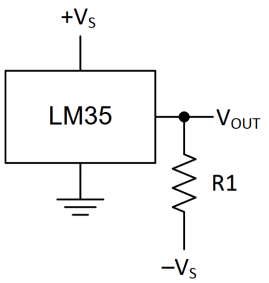

Fig3.1 - LM35 Circuit - V_s = 5 V and R_1 = 100 kΩ in our case.

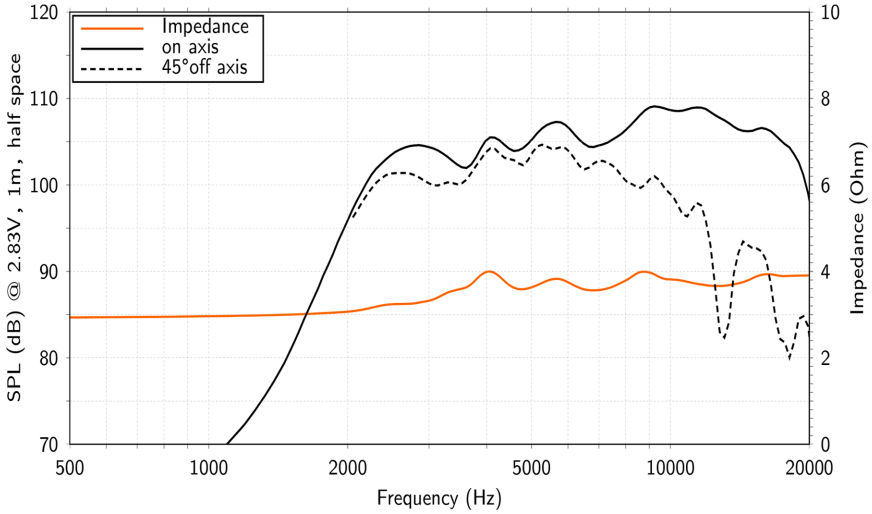

Fig.3.2 - Speaker Frequency Response

IV Measurements & Data Analysis

In this section we present collected data in a chronological order, starting from earlier functional versions of the system up to the latest and more robust versions from late November and early December 2021. Each experiment is discussed including statistical and qualitative analysis of the obtained data together with comments related to the specific context in which the experiments were carried out.

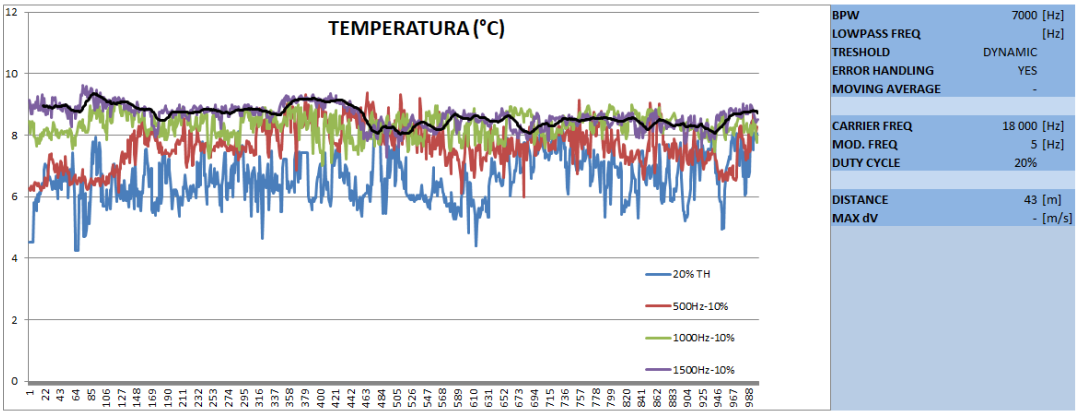

Fig.4.1 - November 3rd 2021 - Four different lowpass frequencies (43 m)

The plots in Fig.4.1 represent subsequent measurements of around 1000 samples at a rate of 5 measurements a second for a total of 200 seconds. The blue measurement was taken with a dynamic threshold of 20% while all the others are at 10%. The lowpass cut-off frequency is increased with each measurement in order (red-green-purple). This result is compatible with our theoretical predictions of the absolute error decreasing as the filter gets wider at the cost of increased noise and nonlinearities added to the demodulated waveform.

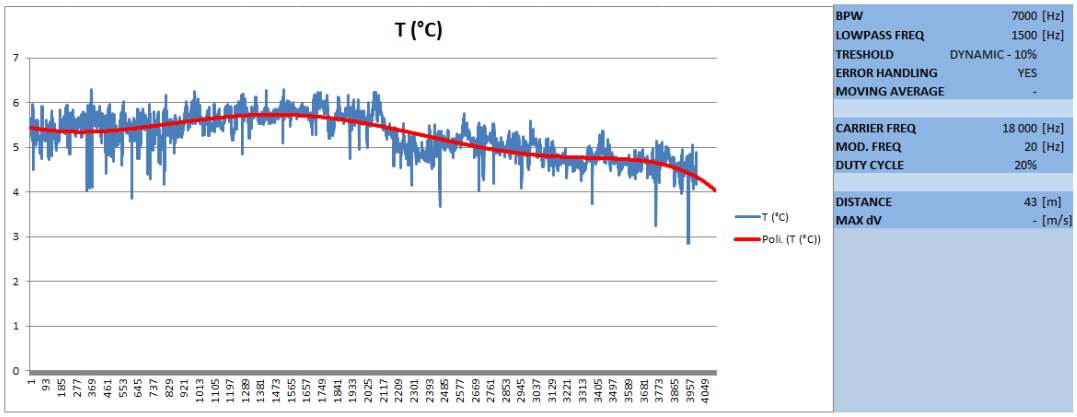

Fig.4.2 - November 4th 2021 - 1500 Hz Lowpass frequency and 20 Hz modulating frequency (43 m)

This measurement does not use Cramer's formula for the temperature conversion, from this point we will specify which measurements include Cramer's while for all the rest it is to be assumed the use of equation (1.1 CH I). A low-pass frequency of 1.5kHz is used and some errors are present due to the lower filtering of disturbances.

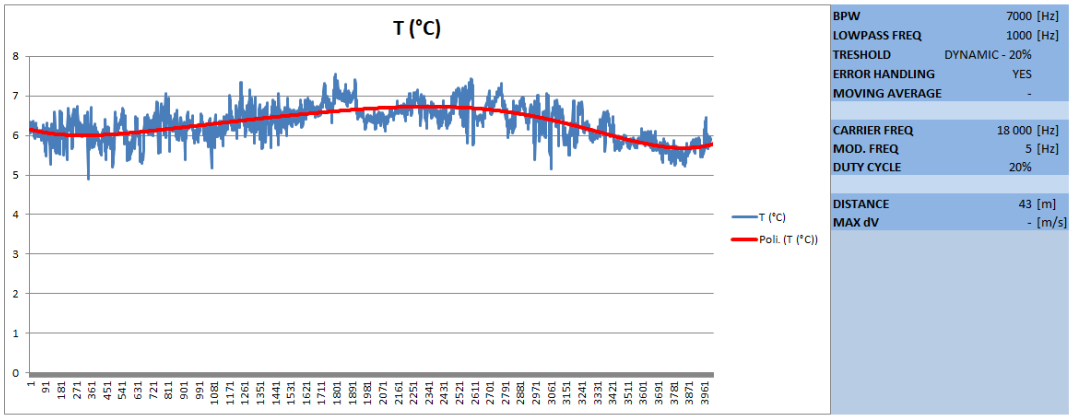

Fig.4.3 - November 4th 2021 - 1000 Hz Lowpass frequency and 5 Hz modulating frequency (43 m)

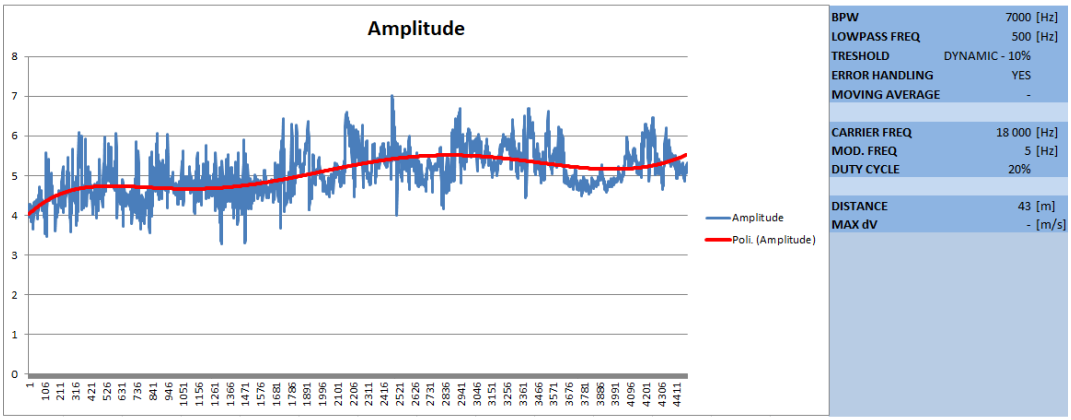

Fig.4.4 - November 4th 2021 - 500 Hz Lowpass frequency and 5 Hz modulating frequency (43 m)

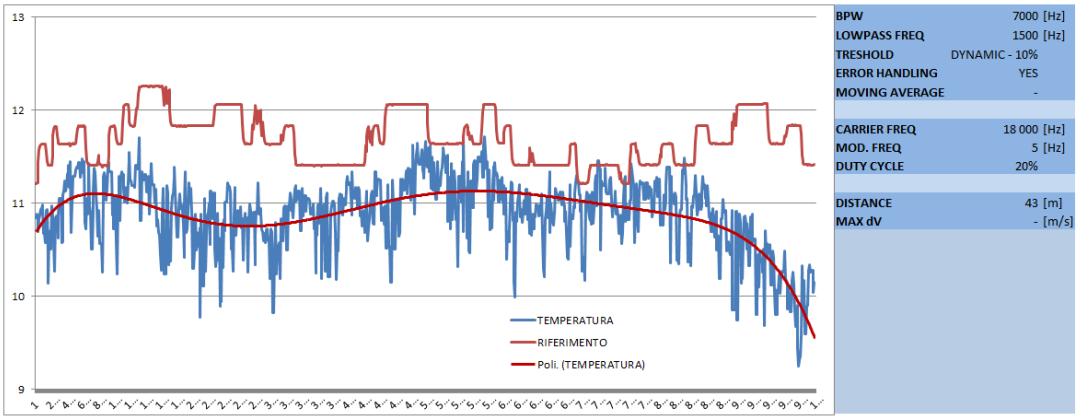

Fig.4.5 - November 5th 2021 - 1500 Hz Lowpass frequency and 5 Hz modulating frequency (43 m). The red line represents the temperature reference.

This measurement combines the temperature reference and measured temperature giving a standard deviation calculated as the average of the roots of the squared difference between each reference and measured sample of $\sigma_m = 0.805$.

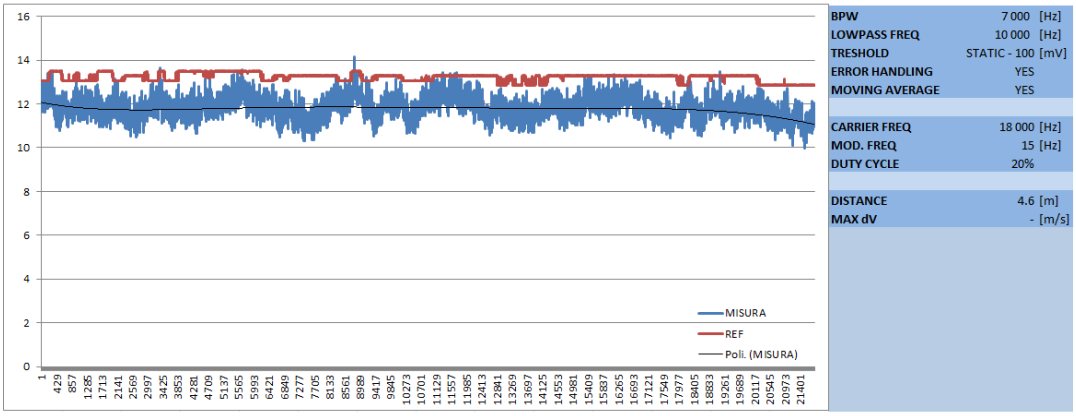

Fig.4.6 - November 11th 2021 - 10000 Hz Lowpass frequency and 15 Hz modulating frequency (4 m)

This measurement took place at a distance of 4.6 meters, requiring a much larger low-pass frequency of 10kHz for a fast response. The uncertainty in distance becomes much more critical at this distance. The standard deviation is $\sigma_m = 1.464$. On the same day a series of measurements were conducted at the same distance and frequencies but varying the low-pass cut-off frequency and calculating for each one the corresponding standard deviation from the reference, the results are found in the following graph.

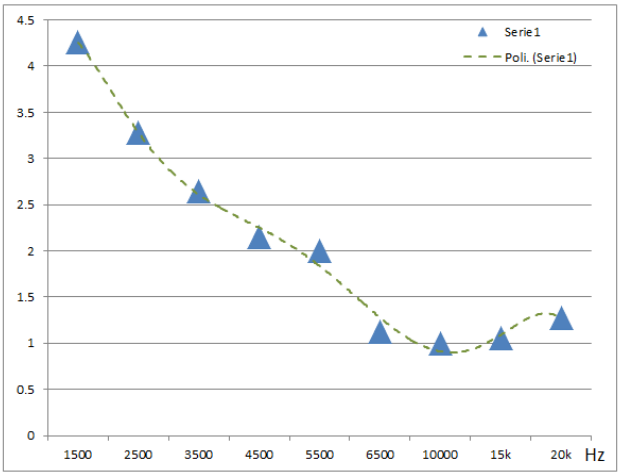

Fig.4.7 - November 11th 2021 - Standard deviations with a varying low-pass cut-off frequency at a distance of 4.6m and a carrier frequency of 18kHz.

The improvement in uncertainty stops at 1K once the cut-off frequency reaches 10kHz, this is to be expected as the demodulated waveform can never switch states faster than the original signal, unless in the presence of disturbances producing timing errors.

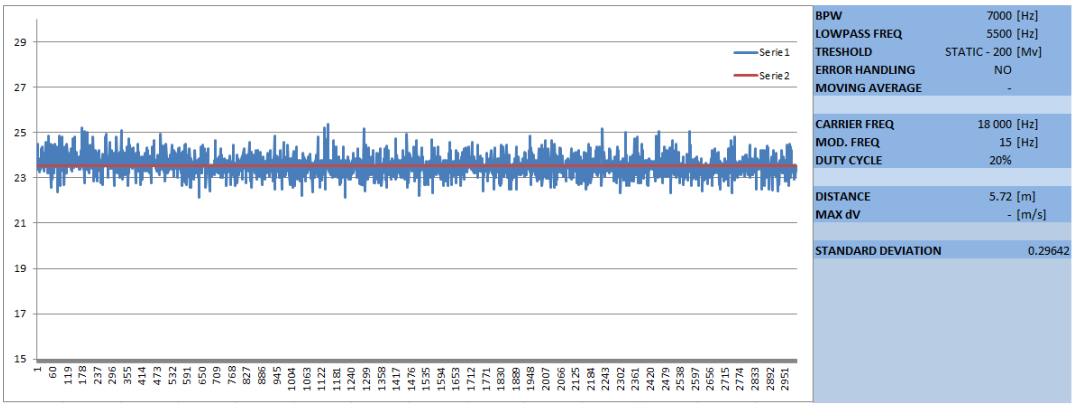

Fig.4.8 - November 15th 2021 - Controlled conditions measurement, 5500 Hz Lowpass frequency and 15 Hz modulating frequency (5.72 m)

To further test the accuracy of our system we decided to conduct a controlled experiment inside our building where the temperature is relatively constant and close to no wind & turbulence is present. At a distance of 5.6m the measurements give a standard deviation with respect to the average of the samples of $\sigma = 0.296$ showing the minimum uncertainty our system is capable of.

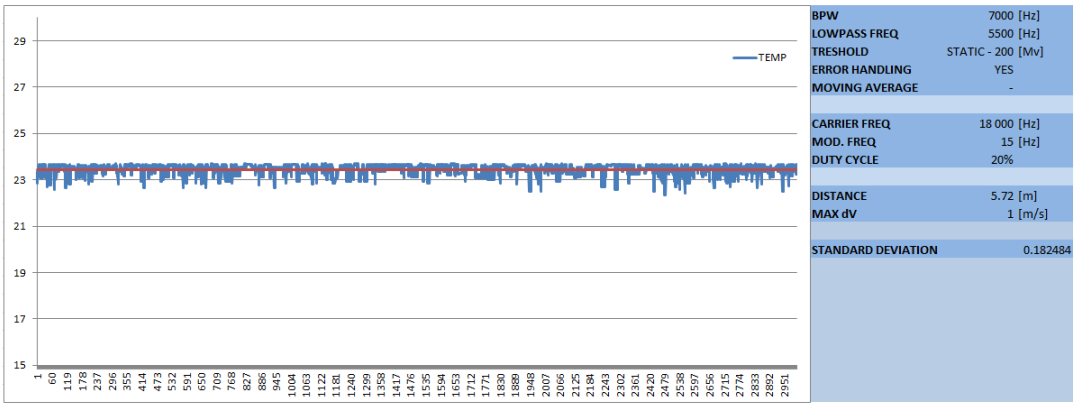

Fig.4.9 - November 15th 2021 - Controlled conditions measurement with enabled error handling algorithm

The second measurement was executed in the exact same conditions expect for enabling the error handling algorithm, the result is more accurate giving a standard uncertainty with respect to the population average of $\sigma = 0.182$.

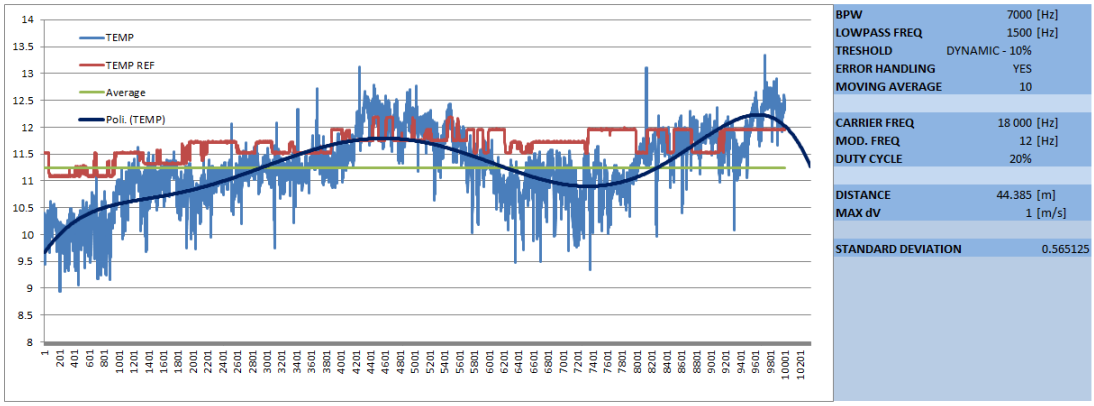

Fig.4.10 - November 16th 2021 - 1500 Hz Lowpass frequency and 12 Hz modulating frequency (44 m)

The system was brought back outside at a distance of 44.6m and another round of experiments were done, the one above (Fig.4.10) is a 13.8 minute measurement giving a standard deviation with respect to the station reference of $\sigma_m = 0.565$.

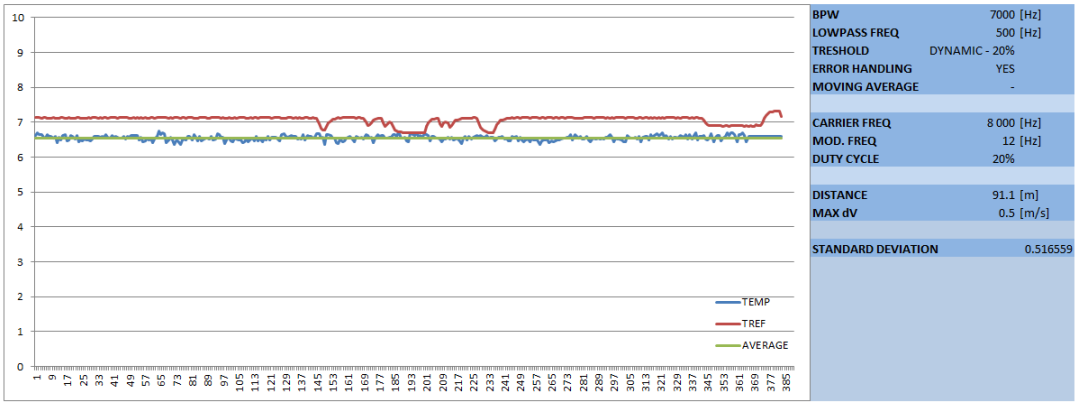

Fig.4.11 - November 19th 2021 - 500 Hz Lowpass frequency and 12 Hz modulating frequency (91.1 m)

On November 19th the system was moved at a distance of 91m for another measurement, this time at a lower carrier frequency of 8kHz with a low pass frequency of 500Hz. The lower carrier frequency was needed after observing that at 18kHz even high transmission powers were not enough to get a meaningful signal on the receiving side, the dissipation in air was excessive at this frequency and could not be worked around at such a large distance. The result shows again a standard deviation of $\sigma_m = 0.516$.

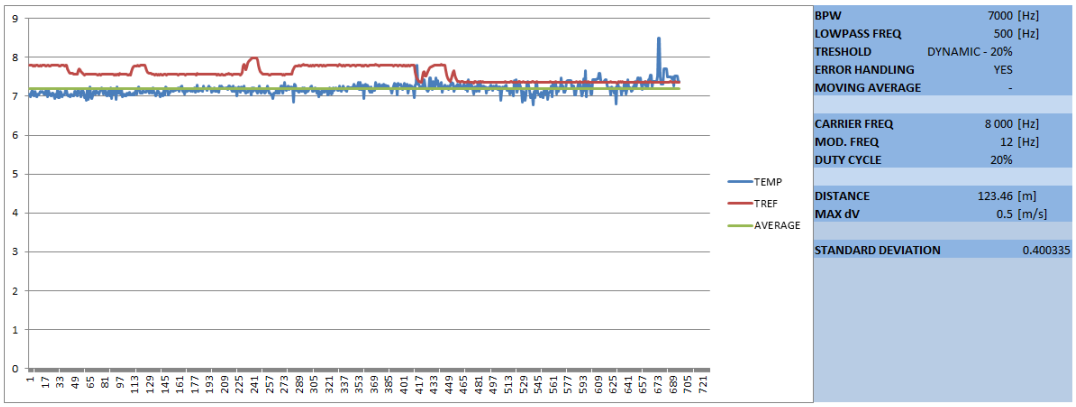

Fig.4.12 - November 19th 2021 - 500 Hz Lowpass frequency and 12 Hz modulating frequency (123.46 m)

On the same day the distance was increased to 123.45m and using the same carrier and low-pass frequencies a standard deviation of $\sigma_m = 0.4$ was obtained over a duration of one minute.

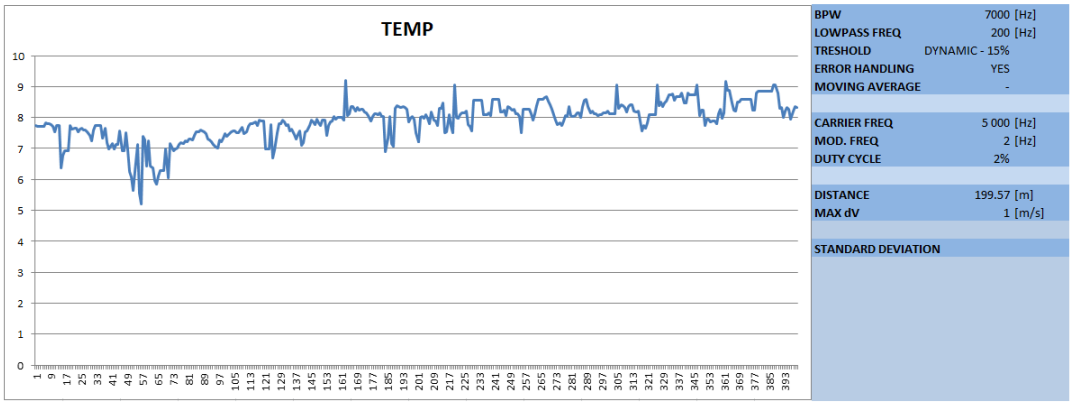

Fig.4.13 - November 26th 2021 - 200 Hz Lowpass frequency and 2 Hz modulating frequency (199.57 m)

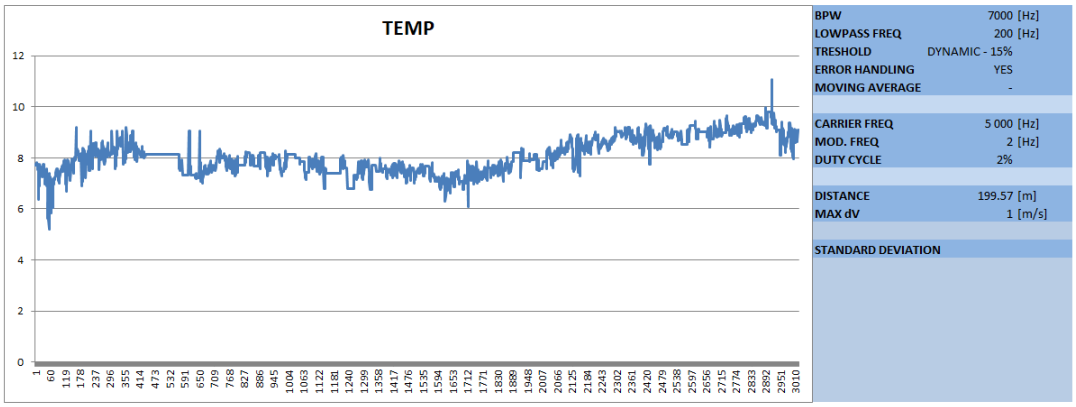

Fig.4.14 - November 26th 2021 - 200 Hz Lowpass frequency and 2 Hz modulating frequency (199.57 m)

A longer measurement took place on November 29th and lasted for over 90 minutes recording two values a second. The standard deviation with respect to it's own moving average (on a 60 second window) of $\sigma = 0.31$.

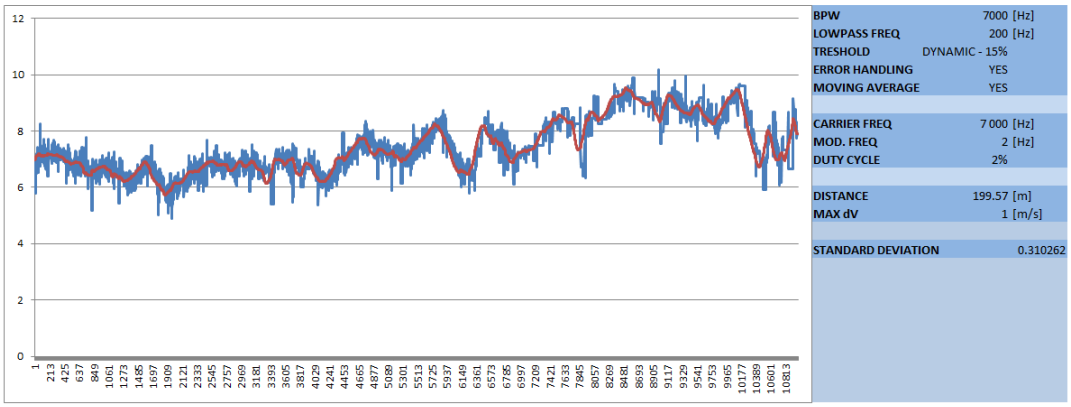

Fig.4.15 - November 29th 2021 - 200 Hz Lowpass frequency and 2 Hz modulating frequency (199.57 m)

Another measurement lasting 60 minutes and started 10:56AM and referenced to the INRiM meteo station showed a standard deviation of the moving average (on a window of 120 values) with respect to the reference of $\sigma = 0.4$.

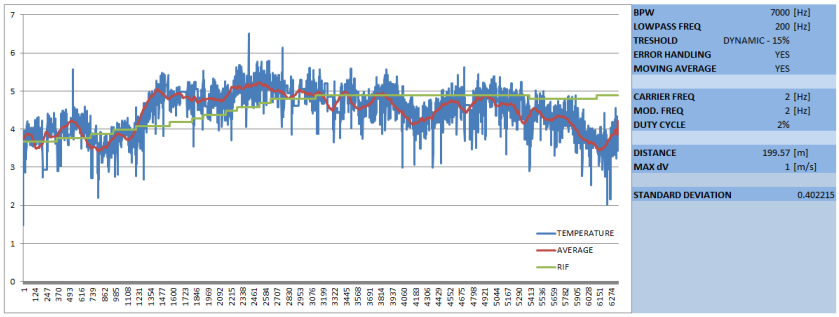

Fig.4.16 - November 30, 2021 - 200 Hz Lowpass frequency and 2 Hz modulating frequency (199.57 m)

The measurement in Fig.4.17 took place between 14:49 of November 30 and 9:30 of December 1st. The blue plot is the temperature taken from the INRiM meteo station at one value per minute, the one in red is the measured temperature at two values per second.

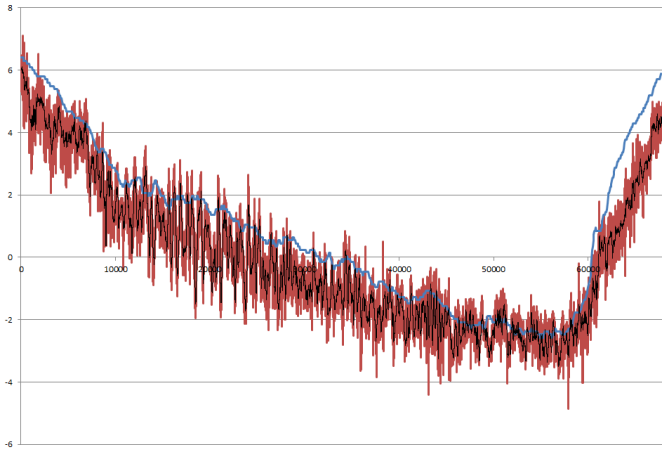

Fig.4.17 - Night of November 30-December 1st, 2021 - 180 Hz Lowpass frequency, 2 Hz modulating frequency with a 6.5kHz carrier (199.57 m)

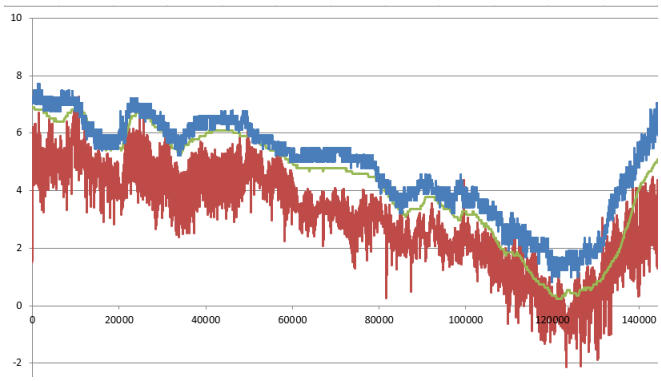

Fig.4.18 - Night of December 1st-2nd, 2021 - Same settings as 4.17 (0.5 second intervals)

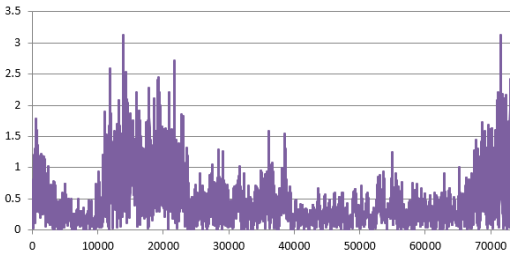

Fig.4.19 - Night of December 1st-2nd, 2021 - Absolute wind speed (1 second intervals)

On the 2nd of December the system was brought back in controlled conditions to test the influence of the low pass filter over the time delay. The following is a comparison of the time delays at a controlled temperature of 21.6°C over the low pass frequency range 200-7500Hz. This shows that the system can afford a much lower cut-off frequency at long distances without sacrificing a more precise time delay. All previous measurements were carried out with a third order filter, this promised an improved performance for subsequent measurements by switching to a first order filter.

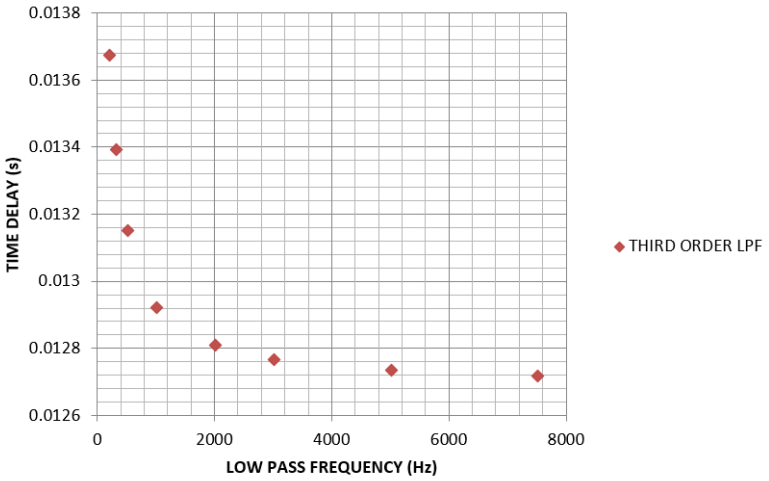

Fig.4.20 - Distance: 4.379m - Third Order Low Pass Filter

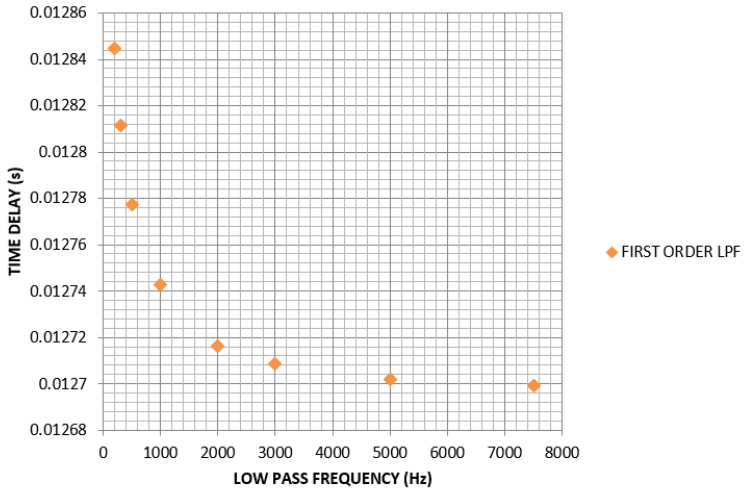

Fig.4.21 - Distance: 4.379m - First Order Low Pass Filter

From the filter measurements we observe that the time delay difference shrinks by one order of magnitude when switching from a 3rd order filter to a 1st order one. Assuming this time delay does not change by a significant margin as a function of carrier frequency, subtracting one millisecond of delay from the measurement in Fig. 4.18 brings a major improvement in uncertainty.

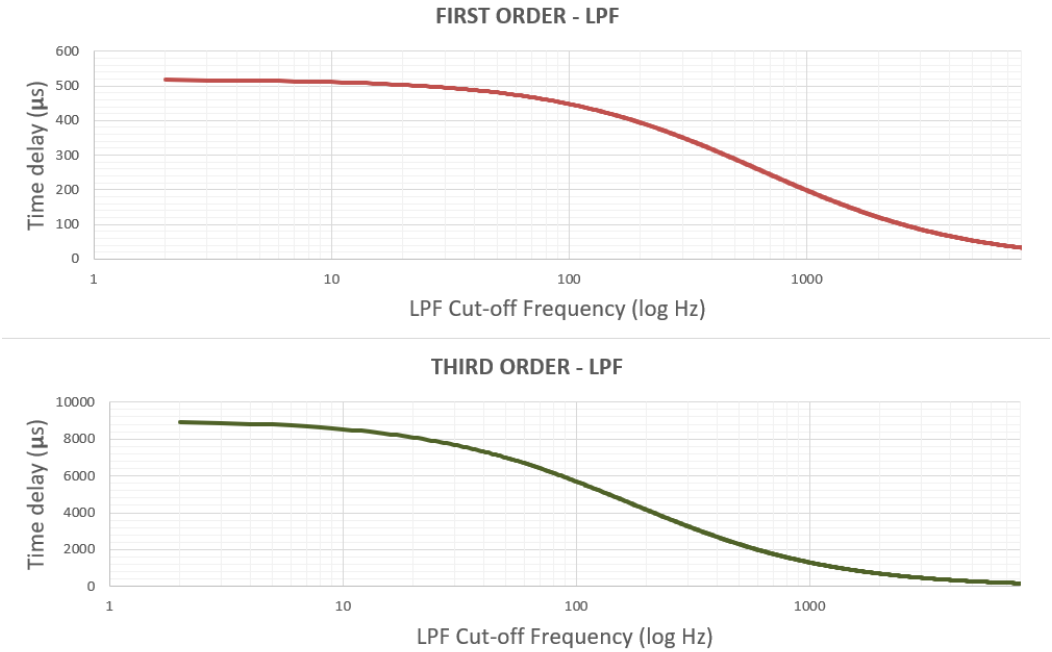

Fig.4.22 - Time delay extrapolation based on the measurements in 4.20/21

Effective acoustic distance correction

Due to the physical geometry of the microphone & speaker pair, there is an intrinsic difference between the distance measured from certain reference points on the objects themselves and the acoustic distance as seen by the system. Two measurements were taken in controlled conditions at a temperature of 22°C, relative humidity of 22% (giving a speed of sound of 344.96m/s). Both the measurements show a constant difference between measured physical distance and the distance seen by the instrument to give the known temperature. This difference turns out to be around 9 cm for the BOYA/NEO microphone-speaker pair when the distance is measured from the first circular opening of the microphone (around 10cm from the microphone tip) and the speaker metal base.

Measured distance (cm)	Measured delay (ms)	Acoustic distance (cm)
30.5	1.15	39.5
95.5	3.03	104.5

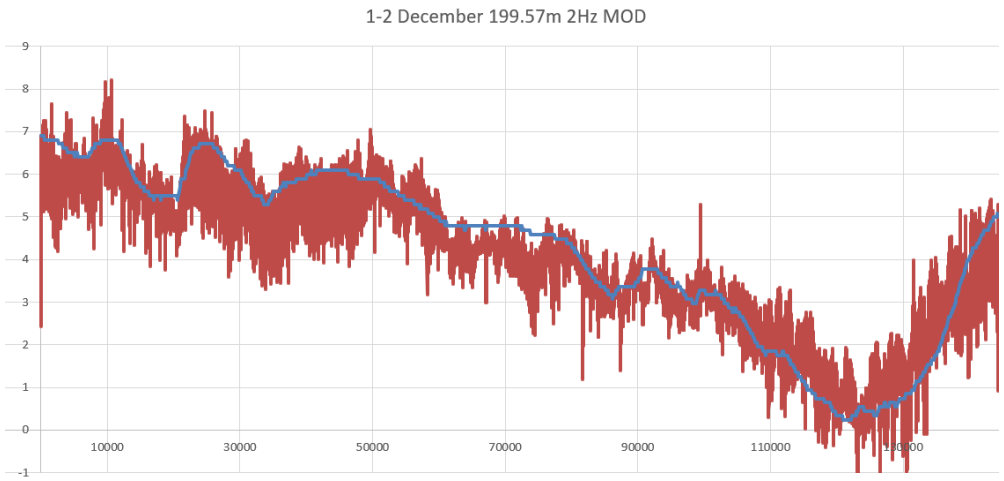

Fig.4.23 - Offset correction for the measurement in fig. 4.18 - The blue plot represents the INRiM station reference.

The last measurement between 18:30 of December 6th and 7:33 of December 7th 2021 was done at a distance of 201m. The moving average of the measured temperature considering windows of more than 120 samples get closer to the reference plot showing that turbulence and wind may cause temperature drifts but the random nature of those disturbances make their average still follow a reference temperature very closely (an error of less than 1K most of the time). We remind again that the two systems measure a different physical quantity and thus differences are to be expected.

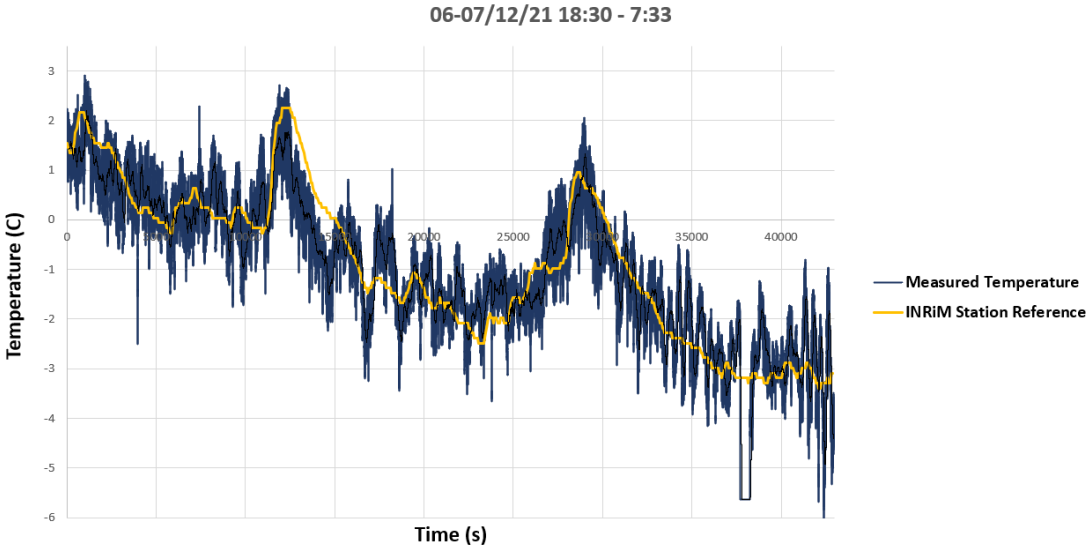

Fig.4.24 - Distance: 201m - Carrier Frequency : 6.5kHz - Modulating Frequency: 2Hz - Low Pass Filter : 50Hz

V Conclusion

The acoustic thermometer in this paper provides a temperature uncertainty under one Kelvin and a drift from local temperature references of less than 2K in all test conditions. Considering that a local classical thermometer measures it's own temperature at more or less one point in space, the systematic constant errors present with respect to this acoustic thermometer are to be expected as the actual measurement is that of a speed of sound over a large mass of moving & turbulent air. The outcome of the measurement is a temperature taking into account all local air conditions which may vary by a substantial amount over the distances considered. The intrinsic uncertainty in controlled conditions turned out to be around 0.3K without the error correction algorithm and 0.18K in the other case. A detailed comparison with other instruments of this kind is yet to be done as of December 2021.

VI References

[1] L. Nijs and C.P.A. Wapenaar "The influence of wind and temperature gradients on sound propagation, calculated with the two-way wave equation" Delft University of Technology 1989

[2] Owen Cramer "The variation of the specific heat ratio and the speed of sound in air with temperature, pressure, humidity, and CO2 concentration" The Journal of the Acoustical Society of America, Volume 93, Issue 5, May 1993, pp.2510-2516

[3] Lindsay Hannah "Wind and Temperature Effects on Sound Propagation" 2007